

1 **This article is a preprint published at EarthArXiv**

2 **Notice - From the AMS Copyright Policy section 7c: This work has been accepted to the**  
3 **Journal of Climate: <https://doi.org/10.1175/JCLI-D-20-0452.1>. The AMS does not guar-**  
4 **antee that the copy provided here is an accurate copy of the final published work. Copy-**  
5 **right in this work may be transferred without further notice. Copyright and all rights**  
6 **therein are maintained by the author(s) or by other copyright owners. It is understood**  
7 **that all persons copying this information will adhere to the terms and constraints invoked by**  
8 **each author's copyright. This work may not be reposted without explicit permission of the**  
9 **copyright owner. [https://www.ametsoc.org/index.cfm/ams/publications/ethical-guidelines-](https://www.ametsoc.org/index.cfm/ams/publications/ethical-guidelines-and-ams-policies/ams-copyright-policy)**  
10 **and-ams-policies/ams-copyright-policy**

11 **Terrestrial evaporation and global climate: lessons from Northland, a planet**  
12 **with a hemispheric continent**

13 Marysa M. Laguë\*

14 *Department of Earth and Planetary Science, University of California Berkeley, Berkeley, CA,*  
15 *USA, and University of Saskatchewan Coldwater Lab, Canmore, Alberta, Canada*

16 Marianne Pietschnig

17 *Department of Mathematics, University of Exeter, Exeter, United Kingdom*

18 Sarah Ragen

19 *School of Oceanography, University of Washington, Seattle, WA, USA*

20

Timothy A. Smith

21

*Oden Institute for Computational Engineering and Sciences, The University of Texas at Austin,*

22

*Austin, TX, USA*

23

David S. Battisti

24

*Department of Atmospheric Sciences, University of Washington, Seattle, WA, USA*

25

*\*Corresponding author address: Marysa M. Laguë, Department of Earth and Planetary Science,*

26

*University of California Berkeley, 307 McCone Hall, Berkeley, CA 94720.*

27

*E-mail: [mlague@berkeley.edu](mailto:mlague@berkeley.edu)*

## ABSTRACT

28 Motivated by the hemispheric asymmetry of land distribution on Earth, we  
29 explore the climate of Northland, a highly idealized planet with a Northern  
30 Hemisphere continent and a Southern Hemisphere ocean. The climate of  
31 Northland can be separated into four distinct regions: the Southern Hemi-  
32 sphere ocean, the seasonally wet tropics, the mid-latitude desert, and the  
33 Great Northern Swamp. We evaluate how modifying land surface proper-  
34 ties on Northland drives changes in temperatures, precipitation patterns, the  
35 global energy budget, and atmospheric dynamics. We observe a surprising  
36 response to changes in land-surface evaporation, where suppressing terres-  
37 trial evaporation in Northland cools both land and ocean. In previous studies,  
38 suppressing terrestrial evaporation has been found to lead to local warming  
39 by reducing latent cooling of the land surface. However, reduced evaporation  
40 can also decrease atmospheric water vapor, reducing the strength of the green-  
41 house effect and leading to large-scale cooling. We use a set of idealized cli-  
42 mate model simulations to show that suppressing terrestrial evaporation over  
43 Northern Hemisphere continents of varying size can lead to either warming  
44 or cooling of the land surface, depending on which of these competing effects  
45 dominate. We find that a combination of total land area and contiguous con-  
46 tinent size controls the balance between local warming from reduced latent  
47 heat flux and large-scale cooling from reduced atmospheric water vapor. Fi-  
48 nally, we demonstrate how terrestrial heat capacity, albedo, and evaporation  
49 all modulate the location of the ITCZ both over the continent and over the  
50 ocean.

## 51 **1. Introduction**

52 The physical properties of the land surface and the ocean differ in several fundamental ways. For  
53 instance, land has a much lower heat capacity than ocean (Cess and Goldenberg 1981; North et al.  
54 1983; Bonan 2008); land has a higher albedo than ocean (Budyko 1961, 1969; Payne 1972; Bonan  
55 2008); the ocean has the ability to move heat laterally (Loft 1918; Richardson 1980; Trenberth  
56 and Caron 2001; Ferrari and Ferreira 2011; Forget and Ferreira 2019); and there are large climatic  
57 impacts of terrestrial orography (Queney 1948; Eliassen and Palm 1960; Manabe and Terpstra  
58 1974; Held et al. 1985; McFarlane 1987). Moreover, land stores and evaporates less water than  
59 ocean, and soil and vegetation properties provide resistance to evaporation over land (Manabe  
60 1969; Bonan 2008, and references therein). The contrast between physical properties of land and  
61 ocean are important controls on atmospheric dynamics, profoundly impacting the climate. The  
62 hemispheric asymmetry in land-sea distribution has implications for global climate, including the  
63 higher sensitivity of the Northern Hemisphere to increases in anthropogenic greenhouse gases  
64 (Manabe et al. 1991; Stouffer et al. 1989). In this study, we focus on how the limited capacity of  
65 the land to hold water, its small heat capacity, and its higher albedo alter the climate system.

66 The albedo of different land types is much higher than that of ice-free ocean. Land albedo ranges  
67 from 0.05-0.25 (vegetated) to 0.5-0.9 (glaciers and snow) (Wiscombe and Warren 1980; Oke 1987;  
68 Bonan 2008). In contrast, the surface albedo of the ice-free ocean is generally less than 0.1 (Jin  
69 et al. 2004). The difference in top-of-atmosphere (TOA) albedo between land and ocean is less  
70 drastic, with TOA albedo ranging from 0.25 to 0.6 over snow-free land, and 0.1 to 0.5 over ice-free  
71 ocean for Earth in the present climate. These higher values result from atmospheric controls on  
72 the TOA albedo, via the effects of cloud cover, aerosols, and attenuation (Donohoe and Battisti  
73 2011).

74 Additionally, land has a much smaller heat capacity than the ocean, and a limited ability to  
75 move energy laterally. Oceans can absorb large amounts of energy (Kuhlbrodt and Gregory 2012;  
76 Cheng et al. 2017) and transport energy via ocean currents; there are areas of the ocean that can  
77 continually take up energy, while other regions act as a source of energy to the atmosphere (e.g.  
78 Marshall and Zanna 2014; Forget and Ferreira 2019). In contrast, energy absorbed at one location  
79 on land must be released back to the atmosphere at that same location in the form of upwards  
80 longwave radiation, sensible heat, or latent heat (evaporation). While the land can store energy  
81 on seasonal timescales, the seasonal storage of heat by the land surface is much smaller than that  
82 of the ocean (Marshall and Plumb 2008). The annual mean heat storage of a land surface in  
83 equilibrium is near-zero (Budyko 1974; Milly and Shmakin 2002).

84 The limited capacity of the land surface to hold water and the increased resistance to evapo-  
85 ration over land surfaces compared to over open water drastically alters evaporative fluxes over  
86 land. Over the ocean, evaporation is determined mainly by the meteorological conditions at the  
87 atmosphere-ocean interface (e.g. the surface temperature and atmospheric humidity). In contrast,  
88 dry land surfaces have little water available for evaporation, and thus little evaporation occurs re-  
89 gardless of the evaporative demand of the overlying atmosphere. Various properties of soil and  
90 vegetation further modulate the availability of water to the atmosphere, including total leaf area  
91 and roots that can provide access to water deep in the soil column (Canadell et al. 1996; Bonan  
92 2008). Moreover, plants directly regulate the movement of water from the land to the atmosphere  
93 by opening and closing their stomata (small pores on leaves which modulate gas exchange) (Sellers  
94 et al. 1996).

95 These fundamental physical differences between land and ocean result in very different surface-  
96 atmosphere interactions. Changes in land surface properties can modify the global climate system  
97 (Charney 1975; Shukla and Mintz 1982; Sud et al. 1988; Davin et al. 2010; Laguë et al. 2019).

98 Large hemispheric energy imbalances, such as those generated by sea ice, large-scale vegetation  
99 change, or an idealized energy source can drive large-scale changes in the location of the zonal  
100 mean Intertropical Convergence Zone (ITCZ) and the Hadley circulation (Chiang and Bitz 2005;  
101 Broccoli et al. 2006; Kang et al. 2008; Swann et al. 2012; Laguë and Swann 2016; Kang 2020).  
102 In response to a hemispheric energy imbalance, the rising branch of the Hadley circulation moves  
103 towards the energy-rich hemisphere, thereby moving energy towards the energy-poor hemisphere  
104 and shifting the ITCZ towards the energy-rich hemisphere (Donohoe et al. 2013), provided there  
105 are no large changes in gross moist stability (see Geen et al. 2020, and references therein). The  
106 distribution of land impacts climate in myriad ways, including by directing storm tracks, shap-  
107 ing ocean circulation, generating planetary waves, and impacting orographic forcing and diabatic  
108 heating of the atmosphere (Eliassen and Palm 1960; Hartmann 1994; Donohoe et al. 2020).

109 At present, 68% of land on Earth is in the NH and 32% is in the SH. The hemispheric asymmetry  
110 in this distribution of land has long been thought to drive asymmetries in surface temperature  
111 (Croll 1870; Stouffer et al. 1989; Manabe et al. 1991), precipitation and ocean heat transport  
112 (Nilsson et al. 2013). In this study we investigate the climatic implications of the asymmetry  
113 in the distribution of land between the Southern Hemisphere (SH) and the Northern Hemisphere  
114 (NH). We use an atmospheric general circulation model configuration to explore how fundamental  
115 differences between the land and ocean affect the climate. We model the climate of a hypothetical  
116 planet that is Earth-like in size and orbital configuration, but has an idealized continent covering the  
117 entire Northern Hemisphere, and an ocean covering the entire Southern Hemisphere. We explore  
118 the mean state of this planet, which we call Northland, and probe how modifying the albedo of the  
119 land surface and its capacity to hold water alter the planet's climate. We also explore the climate  
120 of several alternative continental configurations, and consider a land-covered planet.

121 Idealized models are a useful tool in climate science as they help to narrow the gap between  
122 simulating the climate system and understanding its mechanisms, as highlighted in Sellers (1969),  
123 Held (2005), Jeevanjee et al. (2017), and Maher et al. (2019). Idealized models can be traced back  
124 to ‘Galilean’ idealizations, in which a problem is simplified to make it easier to solve (McMullin  
125 1985). While an idealized model sacrifices realistic representations of physical processes, this  
126 approach aides in illuminating fundamental processes of the climate system (Levins 1966) – in  
127 this case, differences between land and ocean surface interactions with the atmosphere.

## 128 **2. Methods**

### 129 *a. Model*

130 We use Isca (Vallis et al. 2018), a framework for designing idealized atmospheric general circu-  
131 lation models (GCMs), to explore the climate of an Earth-like planet with an idealized continental  
132 configuration. The atmosphere is coupled to a 20m slab ocean without any ocean heat transport  
133 in our simulations. Land gridcells differ from ocean gridcells by having a higher albedo, smaller  
134 heat capacity, a finite reservoir of water, and a parameterized representation of soil moisture that  
135 leads to a reduction in evaporation when the soil is less than saturated. The land parameterization  
136 used in this study is similar to that of Manabe (1969), where land hydrology is represented using  
137 a bucket model. In this model configuration, there is no snow or sea ice, thus no representation  
138 of surface albedo feedbacks which would amplify cooling when surface temperatures drop below  
139 freezing; soil moisture does not impact land surface albedo.

140 The atmosphere uses moist dynamics, but does not represent clouds. While cloud responses to  
141 land surface properties and their changes can play an important role in determining impacts on  
142 surface climate (Cho et al. 2018; Sikma and Vilà-Guerau de Arellano 2019; Laguë et al. 2019;

143 Kim et al. 2020), cloud responses to climate perturbations are also a large source of uncertainty  
144 (Stocker et al. 2013; Zelinka et al. 2017). Our idealized modeling framework avoids uncertainties  
145 associated with cloud responses to climate perturbations, at the cost of not capturing any cloud  
146 interaction effects. The surface albedo  $\alpha$  of both water ( $\alpha_{ocean} = 0.25$ ) and land ( $\alpha_{land} = 0.325$ ;  
147 table 1) is higher than it would be in a model that included clouds, to allow for a more realistic  
148 planetary albedo at the top of the atmosphere (Donohoe and Battisti 2011). Despite the absence  
149 of clouds, the model still produces precipitation (see Vallis et al. 2018, for details). Simulations  
150 are run using a T42 horizontal resolution (roughly  $2.8^\circ$  latitude by  $2.8^\circ$  longitude) with 40 vertical  
151 levels.

## 152 *b. Experiments*

153 We run a total of 14 simulations, with six continental configurations and various land surface  
154 properties modified between simulations (table 1). In all simulations, there is a seasonal cycle in  
155 insolation (obliquity = 23.439 degrees, eccentricity = 0) with a 360 day year; atmospheric CO<sub>2</sub>  
156 concentrations are fixed at 300 ppm. We refer to the six continental configurations as “North-  
157 land”, “ThreeQuarterLand”, “NorthWestLand”, “ThreePatchLand”, “TwoPatchLand”, and “Lake-  
158 world”, (figure 1). Lakeworld is entirely land with no ocean, while TwoPatchLand, ThreePatch-  
159 Land, NorthWestLand, ThreeQuarterLand, and Northland have a SH ocean and land covering  
160 between half and all of the NH (see table 1 and figure 1 for details).

161 For the Northland continental configuration, we consider 4 simulations with varied land surface  
162 properties; we refer to these simulations as “NorthlandXX” (where “XX” indicates a specific  
163 simulation). Our “control” simulation (to which we generally compare our other experiments) is  
164 “NorthlandBright”. In NorthlandBright, the NH continent has an albedo that is 1.3 times that of  
165 the ocean ( $\alpha_{land} = 0.325$ ,  $\alpha_{ocean} = 0.25$ ). The heat capacity of the land is 1/10 that of the ocean in



166 our simulations (i.e. equivalent to a 2m mixed layer ocean). This is larger than the heat capacity of  
167 land on Earth, but Isca simulations with realistic continents have been shown to compare well with  
168 reanalyses when these heat capacities are used (Thomson and Vallis 2019; Geen et al. 2018). The  
169 roughness length is 0.2 mm, and is uniform over land and ocean in our simulations. Hydrology  
170 is represented by the “bucket model” (Manabe 1969; Vallis et al. 2018), where the capacity of  
171 the land to hold water (“bucket capacity”) is set to 150 mm in our simulations, and water on  
172 land is initialized everywhere at 100 mm. The bucket receives water when precipitation exceeds  
173 evaporation and loses water when the opposite occurs. When the bucket is more than 3/4 full, the  
174 resistance to evaporating water from the land surface is the same as over open water. When the  
175 bucket is less than 3/4 full, evaporative resistance scales inversely with the amount of water in the  
176 bucket.

177 We run three additional Northland experiments to demonstrate various aspects of the land sur-  
178 face’s impact on the climate system. In each of these simulations, a single property of the land  
179 surface is modified compared to NorthlandBright. In the “NorthlandDark” experiment, the albedo  
180 of the land is reduced so that it is the same as the ocean ( $\alpha_{land} = \alpha_{ocean} = 0.25$ ). In the “North-  
181 landEmpty” experiment, the land surface is initialized with no water on the land surface; thus, all  
182 water that ends up on land must have originated from the SH ocean. NorthlandEmpty differs from  
183 NorthlandBright only in the initial conditions. In the “NorthlandDry” experiment, the capacity  
184 of the land to hold water is greatly reduced, to near-zero (0.01 mm). This effectively shuts off  
185 evaporation from the land surface.

186 For each of the NorthWestLand, ThreeQuarterLand, TwoPatchLand, and ThreePatchLand con-  
187 tinental configurations, we run two simulations. In “NorthWestLand”, “ThreeQuarterLand”,  
188 “TwoPatchLand”, and “ThreePatchLand”, the land surface has the same properties as Northland-  
189 Bright. In “NorthWestLandDry”, “ThreeQuarterLandDry”, “TwoPatchLandDry”, and “ThreeP-

190 atchLandDry”, the land surface has the same properties as NorthlandDry (i.e. terrestrial evapora-  
191 tion is suppressed).

192 We run one simulation where the entire planet is covered with land. We refer to this simulation as  
193 “Lakeworld”. Lakeworld has the same albedo as NorthlandBright ( $\alpha_{land} = 0.325$ ), but the bucket  
194 hydrology is modified to allow the land to form lakes over gridcells that receive precipitation when  
195 the bucket is already full. When the soil moisture is less than 150 mm, the same rules governing  
196 terrestrial evaporation in NorthlandBright apply. However, the soil is allowed to accumulate an  
197 infinite amount of water. When the soil moisture exceeds 150 mm, the same rules of evaporation  
198 for fully saturated soils (which in these simulations are the same as the rules for open water) apply.  
199 The lakes do not impact land albedo or heat capacity. Lastly, we run an aquaplanet simulation  
200 (“Aqua”) with no land, where the whole planet is covered with a 20m deep mixed layer slab  
201 ocean, with an albedo of  $\alpha_{ocean} = 0.25$ .

202 Most simulations were run for 20 years, though some Northland simulations were run for 50  
203 years to check model drift, and Lakeworld was run for 80 years due to the unique water cycle of  
204 the all-land planet. The first four years of each simulation are discarded to allow for model spin-  
205 up, after which time there is a global-mean drift in surface temperatures of less than 0.01 K/year  
206 in the Northland and Aqua simulations (figure S1). Unless otherwise stated, the results presented  
207 here are taken from years 5-20 of the simulations (5-80 for Lakeworld). The Lakeworld simulation  
208 does not reach equilibrium in 80 years (figure S1), but this simulation is used to demonstrate the  
209 transient migration of water, rather than explored for its equilibrium climate.

210 When statistical significance is shown for a difference between two experiments, a student’s  
211 t-test is used, with  $p < 0.05$  indicating 95% confidence that the simulations differ significantly.  
212 When error bars are used, they represent  $\pm 1$  standard deviation. Analysis was conducted using

213 the Python programming language, heavily leveraging the Numpy (Harris et al. 2020) and xarray  
214 (Hoyer and Hamman 2017) packages.

### 215 **3. Results**

216 Here our goal is to explore the factors that control the surface energy and hydrologic budgets of  
217 the idealized Northland planet. We begin with an overview of the climatology in the Northland-  
218 Bright experiment (section a), which we view as a control simulation. We then investigate how  
219 changes in land albedo (section b) and terrestrial evaporation (section c) impact the temperature  
220 and water cycle of the planet. Next, we explore the effect of suppressing terrestrial evaporation  
221 with alternate configurations that include some ocean in the NH (section d). Finally, we explore  
222 the role of moisture transport (section e), and show that the mere presence of a continent causes  
223 the ITCZ to extend farther poleward than in a pure aquaplanet setting (section f).

#### 224 *a. NorthlandBright (control simulation) climatology*

225 NorthlandBright can be divided into four distinct climatic zones: the SH ocean, the seasonally  
226 wet tropical land belt, the NH mid-latitude desert, and the NH moist high-latitude region. The  
227 mean climate of the NorthlandBright simulation reflects a world where the area-weighted annual  
228 mean surface temperature over the continent is slightly cooler (277K) than over the ocean (280K)  
229 (table S1); this is unlike present-day Earth, where – in the extra-tropics – land regions are generally  
230 slightly warmer than ocean regions (Wallace et al. 1995; Sutton et al. 2007). The continent has  
231 a much larger seasonal cycle of temperature than the ocean, reflecting its smaller heat capacity  
232 (figure 2, table S1). The hottest part of the continent, with temperatures reaching 304K, occurs  
233 around 30°N during NH summer, while temperatures near the North Pole plunge to 220K during  
234 NH winter (figure 2a). Temperatures and seasonality over the SH ocean are much more moderate,

235 with a hemispherically averaged temperature difference of only 4K between summer and winter,  
236 compared to 34K in the NH (table S1).

237 The globally averaged annual mean rainfall in the NorthlandBright simulation is approximately  
238 2 mm/day. Unsurprisingly, more of this rain falls over the ocean (2.9 mm/day) than over the  
239 continent (1.5 mm/day), with a strong latitudinal dependence (figure 2b). The ITCZ has a strong  
240 seasonal cycle, with heavier rainfall and a peak that extends farther polewards over the ocean than  
241 over the continent (figure 2b, 3a). Over the continent, the ITCZ reaches its farthest poleward  
242 extent during August and September, with the peak in precipitation reaching approximately 15°N.  
243 In contrast, the peak in the ITCZ over the ocean occurs at around 20°S during March, with roughly  
244 double the rate of precipitation in the ocean ITCZ-peak than the land ITCZ-peak. The land cannot  
245 support as strong an ITCZ because much of the moisture for the ITCZ must initially be brought  
246 onto the land each season by ITCZ precipitation; in contrast, the ocean provides an unlimited  
247 supply of water in the form of local evaporation that can subsequently be precipitated in the SH  
248 ITCZ.

249 Terrestrial tropical precipitation is most intense from August to November. The land water evap-  
250 orates quickly in the tropics due to high insolation (i.e. evaporation has a similar seasonal cycle to  
251 precipitation; figure 3a-c). North of 20°N, precipitation is roughly equal to evaporation in the an-  
252 nual mean (not shown). Despite heavy wet-season precipitation in the tropics, the ground between  
253 0-20°N dries out during the dry season (February-June), because of strong seasonal evaporation  
254 (figure 3b,d).

255 In the subtropics of the land hemisphere (roughly 20-40°N) there is a desert with dry soil year-  
256 round (figures 2b, 3d). Extratropical precipitation in the land hemisphere features a broad maxi-  
257 mum in NH summer that extends from 50°N to the pole that is likely due to localized convection  
258 (figure 2b). In the ocean hemisphere, the extratropical maximum in precipitation is located at about

259 40°S, and is storm track precipitation associated with baroclinic cyclones (figure 2b). Precipitation  
260 in the ocean hemisphere storm track is nearly seasonally invariant.

261 The high latitude soil is saturated or nearly saturated with water year-round, forming what we  
262 call the “Great Northern Swamp” (figure 3d), with slightly less terrestrial water storage during  
263 June-July when evaporation (fueled by increased summer insolation) exceeds precipitation (figure  
264 3c-d). Interestingly, the soil moisture in the Great Northern Swamp is supplied by water transport  
265 from the tropics, and not from local moisture recycling alone. This becomes clear when the land  
266 is initialized without any water (NorthlandEmpty). In this simulation, the high latitude soil water  
267 is indistinguishable from NorthlandBright within 4-5 years (figures 3d-e). The transport of water  
268 to the poles is explored further in section 3e.

### 269 *b. Climate impacts of land albedo*

270 As we would expect, reducing the albedo of the land surface (making the land darker) leads to  
271 surface warming. In NorthlandDark, the land albedo is the same as that of the ocean. As such,  
272 the land hemisphere absorbs more solar energy in NorthlandDark than in NorthlandBright (figure  
273 S2b), leading to greater temperatures year-round (figure 2c). The additional shortwave (SW) ra-  
274 diation absorbed in NorthlandDark compared to NorthlandBright is released to the atmosphere in  
275 the form of longwave (LW) radiation, sensible heat or latent heat (figure S2c-f). Increased temper-  
276 atures and increased water vapor (resulting in similar relative humidity over the continent between  
277 NorthlandDark and NorthlandBright, figure 2e) lead to more downwelling longwave radiation at  
278 the surface (figure S2a). That is, the warming in NorthlandDark is due to increased SW absorption  
279 as well as increased downwelling LW at the surface. NorthlandDark is warmer than Northland-  
280 Bright over both land (+7.4K, figure 2c, table S1) and ocean (+2.4K, figure 2c, table S1), due to  
281 atmospheric transport of water vapor and heat. The continent in NorthlandDark is not only warmer

282 than NorthlandBright – it is also wetter, particularly during the months of August-October, when  
283 the ITCZ is shifted to the north in NorthlandDark vs. NorthlandBright (figure 2d, figure 4a-b).

284 *c. Climate impacts of reduced terrestrial evaporation*

285 NorthlandDry is the same world as NorthlandBright, except evaporation from the land surface  
286 is suppressed. With all else held equal (i.e. the same amount of incoming energy to the land  
287 surface, etc.), this reduction in evaporation from the land surface is expected to lead to greater  
288 surface temperatures. This is because if evaporative cooling is reduced, the energy absorbed by  
289 the surface must be emitted in the form of sensible heat or longwave radiation, both of which  
290 require an increase in surface temperatures. Indeed, both Shukla and Mintz (1982) and Laguë  
291 et al. (2019) find that reducing evaporation from the land surface leads to surface warming over  
292 land.

293 Contrary to previous studies, we find that suppressing evaporation over Northland leads to  
294 cooler, not warmer, surface temperatures. Annual mean temperatures in NorthlandDry are 3.2K  
295 cooler globally, and 4.9K cooler over land than NorthlandBright (figure 2c, table S1). The cold  
296 anomaly is fairly homogeneous over the ocean hemisphere, but is at its greatest during JJA in the  
297 northern subtropics (figure 2c). This is surprising as the latent heat flux over land is greatly re-  
298 duced in NorthlandDry compared to NorthlandBright (figure 5e), which we would expect to lead  
299 to warming. However, suppressing terrestrial evaporation also reduces the amount of water vapor  
300 released to the atmosphere over terrestrial regions. Water vapor is a strong greenhouse gas, and if  
301 atmospheric water vapor is depleted in sufficiently large quantities, the reduction in the amount of  
302 longwave radiation absorbed by the atmosphere and re-emitted down towards the surface would  
303 cause net cooling. Moreover, while the direct warming effect of reducing latent cooling is locally  
304 isolated to the region where evaporation is reduced, the cooling associated with reduced atmo-

305 spheric water vapor is much broader in spatial extent, as the atmosphere can mix water vapor (or  
306 air with reduced water vapor) beyond the locations where terrestrial evaporation was reduced.

307 The decrease in atmospheric water vapor (figure 2f) due to reduced evaporation from the land  
308 surface cools NorthlandDry relative to NorthlandBright by reducing downwelling longwave radi-  
309 ation (figure 5a). This reduction in downwelling longwave radiation greatly exceeds the reduction  
310 in latent heat flux (which on its own would lead to warming). The reduction in downwelling long-  
311 wave radiation reaches  $150 \text{ W/m}^2$  in the northern high latitudes, while the reduction in latent heat  
312 flux peaks at around  $80 \text{ W/m}^2$ , with the largest reductions in the northern tropics and high latitudes  
313 (compare figure 5a with 5e). In the dry subtropics, the latent heat flux is already near-zero for most  
314 of the year in NorthlandBright, so suppressing evaporation has little impact on temperature in this  
315 region (figure 5e). Hence, cooling is strongest in the dry subtropics, particularly during JJA (figure  
316 2c), because the cooling due to the reduction in downwelling longwave from reduced atmospheric  
317 water vapor has no warming offset from local reductions in latent cooling. There is actually a  
318 slight increase in net shortwave radiation absorption at the surface over land during NH summer  
319 months due to reduced absorption of shortwave radiation by water vapor (figure 5b). However, the  
320 decrease in the downwards emission of longwave radiation from reduced atmospheric water vapor  
321 dominates the change in absorbed surface energy (figure 5f).

322 At the TOA, there is a substantial reduction in net energy absorbed over the continent from June-  
323 August, and an increase in net energy absorbed at the TOA over the continent from September-  
324 December (figure 6c). These changes are dominated by the change in TOA LW. During NH  
325 summer, more LW is lost from the TOA as a result of a smaller greenhouse effect, and there is  
326 less net SW absorption due to reduced atmospheric water vapor (figure 6). That is, despite the  
327 surface being colder during JJA in NorthlandDry than NorthlandBright, there is still more LW lost  
328 from the TOA in NorthlandDry because of the reduced greenhouse effect. This contrasts with the

329 driver of changes in TOA LW from September-December, when there is overall more energy ab-  
330 sorbed at the TOA in NorthlandDry than NorthlandBright (figure 6c). From September-December,  
331 NorthlandDry has less LW emission from the TOA, reflecting the overall colder conditions in  
332 NorthlandDry compared to NorthlandBright (figure 6b).

333 We can compare the change in land surface temperature over Northland due to suppressed terres-  
334 trial evaporation to an equivalent change in albedo, if we assume land surface temperatures scale  
335 linearly with land surface albedo (as was found in Laguë et al. (2019)). The surface temperature  
336 change between NorthlandDark and NorthlandBright implies a 9.9K increase in land surface tem-  
337 peratures per 0.1 decrease in land surface albedo for our idealized planet (see table S1). We note  
338 that this is much larger than the roughly 2K increase in surface temperatures per 0.1 decrease in  
339 land surface albedo found in Laguë et al. (2019), for a realistic continental configuration in a more  
340 complex model. However, intuitively this value should vary with total land area, land distribution,  
341 and cloud cover (which is not represented in this model), as modifying land albedo will have a  
342 different impact on absorbed SW energy and surface temperatures depending on the presence of  
343 clouds and the location of the albedo change. Moreover, surface albedo changes are largely atten-  
344 uated by the atmosphere on Earth and in more complex models (Donohoe and Battisti 2011); as  
345 such, the 0.1 change in surface albedo between NorthlandBright and NorthlandDark results in a  
346 much larger change in planetary albedo in Isca than a similar surface albedo change on the real  
347 Earth. Applying the 9.9K/0.1 decrease in albedo relationship for Northland to the temperature  
348 change in NorthlandDry vs. NorthlandBright tells us that suppressing terrestrial evaporation over  
349 Northland has the equivalent effect on land surface temperatures as increasing the NH albedo by  
350 0.05 (roughly 14%,  $0.05/0.35$ ).

351 The response of precipitation to suppressed terrestrial evaporation in the NorthlandDry experi-  
352 ment is widespread. In particular, precipitation over the continent decreases almost to zero during



353 August-October, which is the wettest part of the year in NorthlandBright. A very weak ITCZ gen-  
354 erates a small amount of precipitation over the southern edge of the continent in August-October  
355 (figure 4c), while precipitation is very low over the rest of the continent year round. We note  
356 that the structure of the Hadley cell during JJA in NorthlandDry differs from the Hadley cell of  
357 the other simulations presented here (figure S3). NorthlandDry does not have a large source of  
358 moisture over the land surface in the tropics. The ITCZ is very weak during JJA (figure 4c), and  
359 rather than an overturning circulation driven by the release of latent heat, the circulation is driven  
360 by direct thermal heating of the surface. The result is two overturning cells stacked on the equator  
361 during JJA, with the lower cell circulating anti-clockwise and the upper cell circulating clockwise  
362 (figure S3f).

#### 363 *d. Temperature response to suppressed evaporation in various continental configurations*

364 The unexpected cooling of Northland with suppressed terrestrial evaporation is due to the re-  
365 duction in downwards LW from reduced atmospheric water vapor (and thus a weaker greenhouse  
366 effect) dominating any surface warming from reduced latent heat fluxes. Because the Northland  
367 continental configuration has no oceanic water source in the NH, NH atmospheric water vapor  
368 becomes significantly depleted (figure 7o). We further explore the effects of suppressing terres-  
369 trial evaporation on surface temperature by considering four additional continental configurations  
370 with varying amounts of ocean in the NH: TwoPatchLand, ThreePatchLand, NorthWestLand, and  
371 ThreeQuarterLand (figure 1, table 1). We compare simulations where the continents have the same  
372 land surface properties as NorthlandBright (i.e. “normal” land surface properties) to simulations  
373 where the continents have the same land surface properties as NorthlandDry (i.e. terrestrial evap-  
374 oration is suppressed), to explore the trade-off between warming from reduced surface latent heat  
375 flux and cooling from reduced atmospheric water vapor.

376 In TwoPatchLand, suppressing terrestrial evaporation leads to 1.0K of warming over land, on  
377 average (figure 7a, 8a). However, as with the dry regions of NorthlandBright, suppressing evap-  
378 oration over regions that are climatologically dry in TwoPatchLand (i.e. the subtropics) does not  
379 lead to any direct warming through reduced evaporative cooling (figure 7a). Instead, these sub-  
380 tropical land areas experience cooling when terrestrial evaporation is suppressed as a result of  
381 decreased downwards LW from reduced atmospheric water vapor. In NorthWestLand, suppress-  
382 ing evaporation also generally leads to warming over land, with an average warming of 0.7K over  
383 land (figures 7b, 8a). The warming is not as strong in NorthWestLand as in TwoPatchLand when  
384 evaporation is suppressed (figure 7a), despite both continental configurations having the same to-  
385 tal land area and the same latitudinal distribution of land area, with 1/2 of the NH covered by  
386 land. The warming is smaller in NorthWestLand despite a comparable (indeed, slightly smaller)  
387 reduction in terrestrial latent heat flux (figure 8b).

388 ThreePatchLand and ThreeQuarterLand have the same total land area: in both cases 3/4 of the  
389 NH are covered by land. However, suppressing terrestrial evaporation leads to warming of the land  
390 for ThreePatchLand, and cooling of the land for ThreeQuarterLand (figure 8a). The warming of  
391 0.3K over land in ThreePatchLand is smaller than in TwoPatchLand or NorthWestLand, reflecting  
392 the larger reduction in atmospheric water vapor (figure 7i) driven by more land area. In Three-  
393 QuarterLand, the reduction in atmospheric water vapor is large enough to dominate warming from  
394 reduced latent heat flux, resulting in net land cooling of 0.3K (figures 7j,l, 8a). The reduction in  
395 latent heat flux from land is larger in ThreePatchLand than ThreeQuarterLand, but the reduction in  
396 latent heat flux from the ocean is much larger in ThreeQuarterLand than in ThreePatchLand (fig-  
397 ure 8b). The differences between ThreePatchLand and ThreeQuarterLand (and TwoPatchLand and  
398 NorthWestLand) demonstrate that it is not only land area, but also continent size and distribution  
399 that modulates the temperature response to suppressed terrestrial evaporation.

400 The change in terrestrial latent heat flux due to suppressed evaporation over land (figure 8b) is  
401 approximately equal to the latent heat flux from the simulations with “normal” surface properties  
402 (from NorthlandBright), because there is almost no evaporation in the simulations with North-  
403 landDry land surface properties. The single large continents have slightly lower latent heat fluxes  
404 in the “normal” simulations than their patchy counterparts; that is, TwoPatchLand and ThreePatch-  
405 Land have slightly larger terrestrial latent heat fluxes than NorthWestLand and ThreeQuarterLand,  
406 respectively, and thus have slightly larger changes in latent heat flux from land when terrestrial  
407 evaporation is suppressed.

408 However, we note that the average area-weighted change in latent heat flux from the land surface  
409 is of comparable magnitude across all the continental configurations considered here (figure 8b),  
410 while total reduction in terrestrial latent heat flux scales with total land area. For simulations with  
411 the same total land area (e.g. TwoPatchLand and NorthWestLand), the total reduction in terrestrial  
412 latent heat flux is similar, but the surface temperature response differs. The temperature change  
413 driven by suppressing terrestrial evaporation is greater when the contiguous continental area is  
414 larger. This occurs because the atmosphere becomes more depleted in water vapor over a single  
415 large continent than it does over two smaller continents separated by ocean. Thus the water vapor  
416 cooling effect is stronger over larger continents than smaller ones, even if the direct warming due  
417 to reduced latent cooling of the surface is similar.

418 Over the oceans, surface temperatures cool and evaporation is reduced as a result of suppressing  
419 terrestrial evaporation in all the TwoPatchLand, ThreePatchLand, NorthWestLand, ThreeQuarter-  
420 Land, and Northland continental configurations (figure 7). The changes in latent heat flux from  
421 the ocean (blue bars in figure 8b) must be the result of changes in the local oceanic surface energy  
422 budget, mainly over the NH ocean. For example, cooling over the NH ocean in ThreeQuarterLand  
423 is more intense than it is over the NH ocean in ThreePatchLand (figure 7 g vs j), which is consis-

424 tent with a greater reduction in oceanic latent heat flux in ThreeQuarterLand vs. ThreePatchLand.  
425 Despite Northland showing the greatest surface cooling and the greatest global reduction in latent  
426 heat flux, the reduction in oceanic latent heat flux in Northland is small compared to the other  
427 continental configurations (figure 8b). This reflects the fact that most of the temperature change  
428 in Northland occurs over the land hemisphere, and not over the ocean. In the other continental  
429 configurations, much of the reduction in oceanic latent heat flux occurs over the NH, where the  
430 temperature changes and decreases in atmospheric water vapor are greatest (figure 7). The cooling  
431 over the ocean is due to a reduction in atmospheric water vapor from suppressed terrestrial evapo-  
432 ration leading to reductions in downward LW. In turn, cooling over the ocean reduces evaporation  
433 from the ocean due to the Clausius Clapeyron relationship. This generates a weak negative feed-  
434 back on the ocean temperature, but also further reduces the water vapor flux to the atmosphere.  
435 Only in a few ocean regions do we see a slight increase in evaporation (not shown), as might be  
436 expected if drier air was being advected off the continent. However, these regions are not all lo-  
437 cated downstream of the continents; most of the ocean shows a decrease in evaporation due to a  
438 reduced greenhouse effect.

439 We can also consider differences between NorthlandDark and Aqua, as the NH in Northland-  
440 Dark has the same albedo as Aqua but a limited capacity to hold water. On the one hand, one  
441 might expect the NH land surface in NorthlandDark to be warmer than in Aqua because of limited  
442 water available for evaporation (thus potentially less latent cooling of the surface). On the other  
443 hand, reduced atmospheric water vapor in the NH of NorthlandDark compared to Aqua could re-  
444 sult in cooling (due to a weaker greenhouse effect). In the comparison of NorthlandDark to Aqua  
445 however, we are not simply considering differences in water availability; the different NH heat  
446 capacities in NorthlandDark and Aqua also lead to differences in evaporation and surface temper-  
447 atures. The smaller heat capacity over the land surface in NorthlandDark results in a much larger

448 seasonal cycle in surface temperatures, with hotter summers and cooler winters (figure 9d). The  
449 difference in heat capacity also generates big differences in NH evaporation between Northland-  
450 Dark and Aqua, since the available energy at the surface in NorthlandDark is used not only to heat  
451 the surface, but also to evaporate water (figure 9b,e). In NH summer, high surface temperatures  
452 cause a high vapor pressure deficit. Combined with the low heat capacity that requires more en-  
453 ergy to be lost by the land surface as heat or moisture, this drives larger latent heat fluxes from the  
454 high latitude land in NorthlandDark than in Aqua, despite Aqua having effectively unlimited water  
455 to evaporate. Moreover, the larger seasonal cycle in temperature in NorthlandDark vs. Aqua has a  
456 non-linear effect on evaporation; the atmospheric demand for water vapor increases exponentially  
457 with temperature following the Clausius-Clapeyron relationship such that at the same relative hu-  
458 midity the vapor pressure deficit of warmer air is larger than that of cooler air (Hartmann 1994;  
459 Bonan 2016). In the annual mean, the tropics in NorthlandDark are hotter and have lower latent  
460 heat fluxes than Aqua, while in the high latitudes, surface temperatures are lower and evaporative  
461 fluxes are higher. This results in an atmosphere that is drier over the NH in the low latitudes, but  
462 actually less dry over the NH high latitudes in NorthlandDark than Aqua (figure 9c). This is no-  
463 tably different from the TwoPatchLand, ThreePatchLand, NorthWestLand, and ThreeQuarterLand  
464 simulations, but is driven primarily by differences in the heat capacity of land vs. ocean, rather  
465 than differences in water availability/evaporation.

466 In summary, we find that suppressing terrestrial evaporation has a direct local warming effect  
467 on the region of evaporative suppression, by reducing latent cooling of the land surface. However,  
468 suppressing terrestrial evaporation indirectly cools globally by reducing atmospheric water vapor  
469 (a strong greenhouse gas). In the case of TwoPatchLand, NorthWestLand, and ThreePatchLand,  
470 the local warming effect dominates the response in most terrestrial regions, while the dominant  
471 effect over ocean and desert land regions is cooling associated with decreased atmospheric water

472 vapor (figure 8a). However, when evaporation is suppressed over ThreeQuarterLand and North-  
473 land, the atmospheric water vapor effect dominates resulting in cooler surface temperatures over  
474 the oceans and most land areas (figure 8a). Because Northland does not have any ocean in the  
475 Northern Hemisphere, the atmosphere can become much more depleted in water vapor than it  
476 can in the other continental configurations (figure 7o). In TwoPatchLand, NorthWestLand, and  
477 ThreePatchLand, atmospheric water vapor is depleted over the continents, but is replenished over  
478 the ocean at all latitudes, such that the zonal-mean reduction in atmospheric water vapor is much  
479 less than the water vapor reduction in Northland (figure 7, right column). While the reduction in  
480 atmospheric water vapor isn't as large in ThreeQuarterLand as in Northland, it is large enough for  
481 the mean response of land temperatures to be an overall cooling (figures 7j, 8a). We deduce that  
482 the land surface temperature response to reduced terrestrial evaporation is a function of both total  
483 land area (which controls the reduction in terrestrial latent heat flux) and contiguous continent size  
484 (which controls how dry the atmosphere becomes).

#### 485 *e. The role of moisture transport*

486 In all the Northland simulations except NorthlandDry (which can't store water on land), a Great  
487 Northern Swamp forms in the northern high latitudes. In the absence of a large low-latitude water  
488 source, is the Great Northern Swamp sustainable? Here we use an all-land simulation, Lakeworld,  
489 to show that the existence of the Great Northern Swamp relies on atmospheric moisture transport  
490 from the SH ocean in all other Northland experiments. Lakeworld has no ocean; land surface  
491 properties are similar to those in NorthlandBright except that lakes of arbitrary depth are allowed  
492 to form on all gridcells, if precipitation exceeds evaporation.

493 Lakeworld rapidly forms two lakes, one over each pole (figure 3f), which deepen as the simu-  
494 lation progresses. Within a few years, all of the water on Lakeworld - which is initialized with

495 100mm of water in every gridcell - has been transported to the polar high latitudes, and the land  
496 in the tropics is completely dry year-round. The lake edges retreat polewards quickly over the first  
497 35 years, then more slowly as the simulation progresses.

498 In effect atmospheric circulation redistributes water to concentrate it in the polar regions. On  
499 the present-day Earth, the lower branch of the Hadley circulation transports moisture equatorward,  
500 but in Lakeworld the moisture is rapidly mixed poleward by mid-latitude eddies, then trapped too  
501 far poleward for this mechanism of equatorward transport. The atmosphere of Lakeworld is very  
502 dry, with atmospheric moisture isolated to the lower troposphere near the summer pole (figure  
503 S4). Because the atmosphere in Lakeworld is so dry, the greenhouse effect is very weak, causing  
504 Lakeworld to be much colder than the simulations that include some ocean (figure S1, S5). Surface  
505 temperatures in Lakeworld are above the freezing point year round in the lower latitudes, and at  
506 higher latitudes during summer (figure S5).

507 The polar lake in Lakeworld has a much smaller latitudinal extent than the Great Northern  
508 Swamp in the Northland simulations. In the Northland experiments, the southern portion of the  
509 Great Northern Swamp receives moisture (which is ultimately from the SH ocean) from mid-  
510 latitude eddies. This does not occur in Lakeworld, because moisture is trapped at the poles after  
511 the first few years of the simulation. The lake continues to drift poleward over the course of the  
512 Lakeworld simulation. The Lakeworld simulation would have to be run to equilibrium to deter-  
513 mine how far poleward the polar lake will retreat. However, we do not continue the Lakeworld  
514 simulation beyond 80 years as (a) the extent of the polar lake in equilibrium is not the focus of  
515 this study and (b) the atmosphere in an all-land configuration leaks moisture in the current con-  
516 figuration of Isca (figure S6). We also explore an all-land simulation that cannot form lakes (i.e.  
517 it has the same land surface properties as NorthlandBright). Like Lakeworld, that simulation also

518 quickly transports water to the poles, but because runoff is discarded when soil moisture exceeds  
519 the bucket capacity, the simulation rapidly loses water from the system (not shown).

520 *f. Land's influence on ITCZ location*

521 The presence of the Northland continent alters the source of energy to the atmosphere by altering  
522 the net surface flux of SW (both through surface albedo and changes in water vapor), altering  
523 LW absorption in the atmosphere by modulating atmospheric water vapor, and modifying the  
524 seasonal timing of energy absorption and release by the land surface. We find that the ITCZ in  
525 both the NH and SH of all Northland experiments extends farther poleward than in Aqua (with  
526 the exception of NorthlandDry, which has very little precipitation over land), despite the greater  
527 water vapor content in the tropics in Aqua (figures 4, 10e). Less SW is absorbed at the NH surface  
528 in NorthlandBright compared to Aqua because of the high land albedo in NorthlandBright (figure  
529 10c). Except in the northern high latitudes, the atmosphere in NorthlandBright has less water  
530 vapor than the atmosphere in Aqua (figure 10a). NorthlandDark has more water vapor over the  
531 NH than Aqua as a result of the higher air temperatures (figure 10b). Though the albedo of the  
532 NH in NorthlandDark and Aqua are identical, differences in atmospheric water vapor between  
533 the simulations result in changes to the amount of SW reaching the surface (figure 10d). The  
534 presence of the NorthlandDark continent also results in an ITCZ extending farther poleward than  
535 both Aqua and NorthlandBright in the NH (figure 10e). To explain the ITCZ position as a result of  
536 the Northland continent in these experiments, we discuss the differences in the hemispheric energy  
537 imbalance between our simulations below.

538 There is an extensive literature exploring how hemispherically asymmetric sources of energy  
539 to the atmosphere cause the atmosphere to transport energy from the energy-rich hemisphere to  
540 the energy-poor hemisphere, with a corresponding shift in the zonally averaged ITCZ towards the



541 energy-rich hemisphere (Kang et al. 2008; Yoshimori and Broccoli 2008; Fasullo and Trenberth  
542 2008; Donohoe et al. 2013; Geen et al. 2020). The relationship between the magnitude of cross-  
543 equatorial energy transport and the location of the ITCZ has been explored for the modern Earth  
544 system, where the ITCZ shifts 2.4-2.7°S per PW increase in northward cross-equatorial energy  
545 transport (Donohoe et al. 2013). In our idealized simulations, we find a marginally steeper rela-  
546 tionship than Donohoe et al. (2013), with a 3.4° southward shift in the annual mean ITCZ latitude  
547 per PW increase in northward cross-equatorial energy transport (figure 11, S7). Several factors  
548 impact this slope, including the gross moist stability of the model and the influence of cloud cover,  
549 a mechanism which is absent from our experimental framework (Geen et al. 2020; Voigt et al.  
550 2014).

551 The greater poleward extent of the zonally averaged ITCZ location is best explained by com-  
552 paring the NorthlandDark and Aqua experiments, since these two configurations have the same  
553 surface albedo and differ only in the heat capacity and capacity to store water in the NH. We argue  
554 that the primary reason for the greater poleward extent of the ITCZ in the Northland simulations is  
555 the difference in heat capacity between the land and ocean hemispheres, which generates greater  
556 hemispheric energy imbalances than in Aqua – both seasonally and in the annual mean.

557 The lower heat capacity of the NH in NorthlandDark provides less of a buffer to the atmospheric  
558 energy imbalance by storing less energy in the surface relative to Aqua during JJA, and releasing  
559 less energy during DJF (compare  $SFC$  in figure 12f,h and j,l). During JJA, the ITCZ extends farther  
560 poleward over the NH in NorthlandDark than Aqua because the land surface takes up little energy,  
561 resulting in a larger atmospheric energy source  $F_{net} = TOA - SFC$  in NorthlandDark than Aqua  
562 (Geen et al. 2020). During DJF, the ITCZ extends farther poleward over the SH in NorthlandDark  
563 than Aqua because the land surface releases little energy, while in Aqua the ocean releases stored  
564 energy to the atmosphere; thus, the NH atmosphere is more energy-poor in NorthlandDark than

565 Aqua during DJF. The net effect is that the NH atmospheric energy source is much larger in  
566 NorthlandDark than Aqua during JJA, while the NH atmospheric energy source is more negative  
567 during DJF in NorthlandDark than Aqua (compare  $F_{net}$  in figure 12f,h and j,l, table S2).

568 In the annual mean, NorthlandDark has a hemispheric imbalance in  $F_{net}$ , while  $F_{net}$  is symmetric  
569 about the equator in Aqua (table S2). This hemispheric energy imbalance results in an annual mean  
570 transport of energy across the equator from the SH to the NH, consistent with a zonally averaged  
571 ITCZ sitting south of the equator (figure 11). Corresponding to this hemispheric atmospheric  
572 energy imbalance, the ITCZ in NorthlandDark extends much farther poleward than the ITCZ in  
573 Aqua, both seasonally and in the annual mean. In NorthlandBright and NorthlandDry, the ITCZ  
574 extends slightly farther south than in NorthlandDark during DJF because the lower surface albedo  
575 (NorthlandBright) and lower water vapor (NorthlandDry) reduces the total amount of energy taken  
576 up during NH summer and subsequently released in NH winter by the land surface, accentuating  
577 the hemispheric imbalance in the atmospheric energy source that already exists as a result of the  
578 smaller heat capacity of land vs. ocean (figure 12a,c; table S2). Details of the calculations used  
579 for figures 11 and 12 are provided in the supplement.

## 580 **4. Discussion**

### 581 *a. Temperature response to suppressed terrestrial evaporation*

582 With all else held equal, reducing evaporation from the land surface should lead to surface warm-  
583 ing, as the energy formerly used to evaporate water is instead re-partitioned into sensible heat or  
584 emitted longwave radiation. While reducing evaporation from the land surface directly leads to  
585 warming (Shukla and Mintz 1982; Laguë et al. 2019), reducing water flux from the land surface  
586 also impacts atmospheric concentrations of water vapor, a strong greenhouse gas. Given the com-

587 peting effects of reduced evaporative cooling which would lead to warming, and reduced longwave  
588 trapping by atmospheric water vapor which would lead to cooling, we hypothesize that a crossing-  
589 point exists in the temperature response to suppressed land evaporation (figure 13). Starting from  
590 a state of sufficient atmospheric moisture, reducing evaporation from the land surface should ini-  
591 tially lead to surface warming as a result of decreased evaporative cooling of the land surface ((i)  
592 in figure 13). However, as atmospheric water vapor concentration decreases, the strength of the  
593 atmospheric greenhouse effect also decreases, inducing a cooling effect on the surface; the warm-  
594 ing signal from suppressed evaporation competes with the cooling from a reduced greenhouse  
595 effect ((ii) in figure 13). Once atmospheric concentrations of water vapor are sufficiently low, the  
596 cooling effect from the reduced atmospheric greenhouse effect dominates the surface temperature  
597 response ((iii) in figure 13).

598 From our simulations, suppressing evaporation over TwoPatchLand would fit into regime (i),  
599 where reduced evaporation warms the land surface. NorthWestLand falls between regimes (i) and  
600 (ii), where the direct warming effect of reduced evaporation is weaker than in TwoPatchLand, thus  
601 the total warming is more strongly damped by the reduction in atmospheric water vapor. Three-  
602 PatchLand and ThreeQuarterLand bracket the crossing-point of the temperature response (regime  
603 ii), with ThreePatchLand warming slightly and ThreeQuarterLand cooling slightly. Northland  
604 falls firmly into regime (iii), where any direct warming of the surface is more than out-weighed  
605 by cooling from reduced atmospheric water vapor. Generally, larger total land areas fall farther to  
606 the right on this curve; however, for the same total land area (e.g. TwoPatchLand vs. NorthWest-  
607 Land), the continental arrangement with the larger contiguous continent size falls farther to the  
608 right. This occurs because when the continents are broken up, the atmosphere can be replenished  
609 with water vapor when it passes over the ocean, while in the case of a larger contiguous continent,  
610 the atmosphere becomes more depleted in water vapor. We suggest the present-day continental

611 configuration of Earth falls into regime (i), both because the present-day continental configuration  
612 of Earth most closely resembles TwoPatchLand (i.e. there is ample ocean at every latitude), and  
613 because previous modeling studies (e.g. Shukla and Mintz 1982; Laguë et al. 2019) find that re-  
614 ducing terrestrial evaporation leads to surface warming over land. Indeed, the largely zonal flow  
615 of the atmosphere would shift any continental configuration with ocean at each latitude towards  
616 regime (i), as the mixing of dry continental and moist oceanic air would prevent any individual  
617 latitude from becoming overly depleted in water vapor.

618 In our simulations, suppressing terrestrial evaporation in all of our continental configurations  
619 leads to cooling over the ocean. This differs from the results of Laguë et al. (2019), who found  
620 that reduced evaporation with a realistic present-day continental configuration leads to surface  
621 warming over most of the ocean.<sup>1</sup> Differences in the ocean temperature response between Laguë  
622 et al. (2019) and this study could be due to nuances in circulation due to the use of realistic  
623 continental geometry and orography in that study, as well as different intensities of suppressed  
624 terrestrial evaporation. In particular, our idealized Isca simulations do not have any representation  
625 of cloud cover, and cloud responses to changes in terrestrial evaporation can have large climate  
626 feedbacks (Laguë et al. 2019). Reduced terrestrial evaporation can lead to drying of the boundary  
627 layer and a reduction in low cloud cover over land, which in turn increases absorbed SW at the  
628 surface and drives warming in water-limited systems, while changes in terrestrial evaporation can  
629 also lead to cloud changes over ocean regions (Laguë et al. 2019; Kim et al. 2020). Understanding  
630 how the presence of clouds, and the response of clouds to reduced terrestrial evaporation, modify  
631 the temperature response to reduced terrestrial evaporation both on land and globally requires  
632 future study.

---

<sup>1</sup>The Shukla and Mintz (1982) study does not inform on changes over the ocean because they prescribe a fixed SST.

633 Based on our results from TwoPatchLand/ThreePatchLand versus NorthWest-  
634 Land/ThreeQuarterLand (section 3d), we postulate that suppressing terrestrial evaporation  
635 in continental configurations with large amounts of arid land (e.g. polar continents) would have a  
636 much weaker impact on water vapor than continents with moist climates (e.g. in the tropics), and  
637 thus would not generate strong large-scale cooling. We also note that we have tested an extreme  
638 level of reduced terrestrial evaporation here. We do not consider the response of temperature to  
639 smaller reductions in terrestrial evaporation such as those driven by the closure of plants' stomata  
640 in response to increased atmospheric CO<sub>2</sub>, which have been shown to generate terrestrial warming  
641 across CMIP 5 and 6 models (Zarakas et al. 2020).

642 We have explored the temperature response to suppressing terrestrial evaporation over ideal-  
643 ized NH continents; in doing so, we have demonstrated that continental configuration is of ut-  
644 most importance in controlling the temperature response to suppressed terrestrial evaporation. We  
645 have identified the competing effects of suppressing terrestrial evaporation on surface temperature  
646 without any complicating factors driven by cloud responses. These idealized simulations do not  
647 represent cloud cover, thus do not capture either how the presence of clouds may modulate the  
648 surface temperature response to reduced terrestrial evaporation, or how cloud changes in response  
649 to reduced terrestrial evaporation may further influence surface temperatures, both locally over  
650 land and over the ocean. Further study is required to identify the seasonality of this response,  
651 which continental configurations lead to warming vs. cooling, what level of reduction in continen-  
652 tal evaporation is required for warming vs. cooling, and what role clouds play in modulating the  
653 temperature response to reduced terrestrial evaporation.

654 *b. Connections to Snowball Earth*

655 Our results raise the question of how past continental configurations and distributions of water  
656 and vegetation on those continents may have impacted both terrestrial and global paleoclimate  
657 through water vapor feedbacks. What is the distribution of continents that is required such that  
658 decreasing evapotranspiration from the land surface leads to a cooling rather than warming? In  
659 present-day Earth, the greenhouse effect is due mainly to water vapor, and the source of water  
660 vapor is net evaporation in the tropics (equatorward of 35° latitude) which is distributed globally by  
661 the atmospheric circulation. In our TwoPatchLand and NorthWestLand continental configurations,  
662 suppressing terrestrial evaporation results in global-scale cooling through reduced atmospheric  
663 water vapor, though the land surface generally warms due to reduced latent cooling. However,  
664 in our Northland continental configuration, the continent covers the entire hemisphere, which  
665 severely reduces the evapotranspiration of water vapor poleward of the ITCZ in the NH. Further  
666 reducing terrestrial evaporation in the NorthlandDry experiment reduces the greenhouse effect  
667 and causes cooling. In this regard, it is illuminating to consider the Snowball Earth events: global  
668 glaciations during which ice covered the entire surface of the Earth (Kirschvink 1992; Hoffman  
669 et al. 1998). There is evidence for two such events during the Neoproterozoic between 630 and  
670 750 million years ago, and one in the early Paleoproterozoic 2.5 billion years ago (Abbot et al.  
671 2013; Hoffman et al. 2017), when most of the continental land masses were located in the tropics  
672 (see Kump et al. 2004; Worsley and Kidder 1991, and references therein).

673 The Snowball Earth atmosphere is cold and holds little moisture (Voigt et al. 2011; Hoffman  
674 et al. 2017). Past work suggests that paleogeographic continental configurations cause a reduction  
675 in atmospheric water vapor compared to an aquaplanet without continents, increasing direct heat-  
676 ing by decreasing cloud cover (Fiorella and Poulsen 2013). Future work could test the robustness

677 of this result and probe whether past tropical megacontinents were large enough to cause a suffi-  
678 cient reduction in tropical water vapor to cool the tropics and contribute to the onset of Snowball  
679 events (though the dry atmosphere of Snowball Earth is attributed to the cold temperatures and  
680 not vice versa (Voigt et al. 2012; Hoffman et al. 2017)). This reduction in tropical water vapor  
681 would cause even greater cooling in the extratropics as a consequence of reduced atmospheric  
682 energy transport (Rose et al. 2014). If this occurred, cooling by reduced total tropical evaporation  
683 would help explain why Snowball Earth happened. However, reductions in continental precipi-  
684 tation would reduce the rate of silicate weathering, thus allowing for greater CO<sub>2</sub> buildup in the  
685 atmosphere, which would act against the formation of a Snowball Earth event. In addition, past  
686 tropical supercontinent configurations would have had some ocean at each latitude band, more  
687 closely resembling our NorthWestLand or ThreeQuarterLand simulations than our Northland sim-  
688 ulations. Notably, the NorthWestLand and ThreeQuarterLand configurations bracket the transition  
689 from warming to cooling when land evaporation is suppressed, suggesting this process could be  
690 relevant for Pangea-like continental configurations, though we have not explored the effect of  
691 varying the position (e.g. moving the whole continent to the tropics) of the megacontinent here.

692 We note that our NorthlandDry simulation has a similar JJA Hadley cell structure as Snowball  
693 Earth. The lack of moisture on the land surface in NorthlandDry means that over the continent  
694 during NH summer, as in Snowball Earth, the Hadley circulation is dominated by dry dynamics  
695 and produces a much smaller overturning circulation than in the present climate (Voigt et al. 2012;  
696 Voigt 2013).

### 697 *c. Precipitation*

698 In our Northland simulations, we find that the polewards extent of the ITCZ over the ocean  
699 hemisphere is influenced by the existence of the NH continent. Specifically, we find the small

700 heat capacity and lower water vapor concentrations of the NH lead to the ocean hemisphere ITCZ  
701 extending much farther polewards than it does in an aquaplanet simulation. This is similar to the  
702 findings of Bordoni and Schneider (2008) and Wei and Bordoni (2018): that ITCZs in aquaplanets  
703 with shallower slab oceans extend farther polewards due to stronger energy gradients between the  
704 summer and winter hemispheres. Our Northland simulations also demonstrate the importance of  
705 hemispheric asymmetries in surface heat storage.

706 Previous studies have shown how hemispheric energy imbalances drive shifts in the zonal mean  
707 location of the ITCZ (e.g. Chiang and Bitz 2005; Broccoli et al. 2006; Kang et al. 2008; Swann  
708 et al. 2012; Maroon et al. 2016). In the current continental configuration on Earth, zonal mean  
709 changes are not generally representative of regional precipitation change (Byrne and O’Gorman  
710 2015; Kooperman et al. 2018; Atwood et al. 2020). However, given our zonally symmetric conti-  
711 nental distribution in Northland, the energy balance framework is a useful tool for understanding  
712 the seasonal cycle of circulation and the distribution of precipitation.

713 In Earth’s present day continental configuration, roughly 68% of the total land mass is in the  
714 NH while the remaining 32% is in the SH. This work raises the question of how much the present  
715 day continental configuration impacts the ITCZ location via asymmetries in seasonal heat storage  
716 between the hemispheres.

717 The present study ties into previous work exploring the impact of continental land masses on  
718 the climate system. The tropical rain belts with an annual cycle and a continent model intercom-  
719 parison project (TRACMIP, Voigt et al. 2016) showed that the presence of an idealised tropical  
720 continent spanning  $45^\circ$  in longitude generally leads to a decrease in global-mean surface tem-  
721 peratures compared to an aquaplanet in several different GCMs. The authors noted that while  
722 this cooling might be expected from the increase in planetary albedo, the patterns of change are  
723 more complex and probably related to changes in cloud cover. Voigt et al. (2016) used a “jello-



724 continent”, which is essentially a patch of thin (lower heat capacity) ocean with higher albedo and  
725 reduced evaporation. In contrast to our study, there is no limit on water availability for evaporation  
726 over the jello-continent, which would be equivalent to unlimited soil moisture in our experiments.  
727 Simulations with “jello” continents in an Earth-like configuration generally capture the present-  
728 day climate well (Geen et al. 2018; Thomson and Vallis 2019), but might be too idealized for  
729 studying precipitation change in response to CO<sub>2</sub> forcing in some tropical regions such as the  
730 Amazon basin (Pietschnig et al. 2019). While the reduction in evaporation due to the presence of  
731 land leads to cooling in TRACMIP, similar to what we see from Aqua to NorthlandDark or from  
732 NorthlandBright to NorthlandDry, the mechanisms for the cooling are different. First, clouds are  
733 not modelled in Isca but are noted to have an impact of surface temperature patterns in TRACMIP.  
734 Second, the inability of the jello-continent to dry out makes the “warming due to reduced latent  
735 cooling” (figure 13 (i)) less extreme, though at the same time the reduction in atmospheric water  
736 vapor – which would lead to cooling (figure 13 (iii)) – would be expected to be less drastic than in  
737 our study.

#### 738 *d. Relationship to all-land planets*

739 Our Lakeworld simulation rapidly transports all the surface water to the poles. We expect this is  
740 because the climatological equator-to-pole temperature gradient ensures an even greater gradient  
741 in moisture (via the Clausius-Clapeyron relationship), and atmospheric storms transport water  
742 vapor towards the high latitudes where the vapor condenses and precipitates. The condensate  
743 remains at the poles because evaporation is greatly reduced by the cooling resulting from the  
744 reduced greenhouse effect. During summer, some of the high-latitude soil moisture evaporates, but  
745 is locally recycled. In the absence of an efficient mechanism to transport moisture from the poles  
746 towards the equator, all the moisture ends up accumulating in the polar regions. This “leaking” of

747 moisture from the tropics to the poles warrants further study: e.g. how much water does the system  
748 require to maintain a moist tropics? What controls the latitudinal extent of the polar lake? This  
749 distribution of surface water is similar to that on other planets, such as Mars, which has two polar  
750 ice caps (Boynton et al. 2002; Wordsworth 2016; Feldman et al. 2004). While the mechanism by  
751 which the water on Mars is concentrated in its polar regions is unclear (Wordsworth 2016), we  
752 note that this is an intriguing similarity with our all-land simulation.

753 The presence of large topographical features could potentially modify the distribution of water  
754 on a land planet, as it could favour the formation of lakes via runoff into basins rather than at the  
755 poles. The distribution of the lakes would then be controlled by surface topography rather than  
756 atmospheric moisture transport alone, as is the case in our simulations. Indeed, previous studies  
757 of all-land planets that include overland river-like mechanisms to bring water back from the high  
758 latitudes to the low latitudes have high soil moisture outside of the polar regions and precipitation  
759 maxima in the mid latitude storm tracks (e.g. Kalidindi et al. 2018), unlike our Lakeworld simula-  
760 tion which has soil moisture maxima at the poles. In their land-planet simulation, Kalidindi et al.  
761 (2018) find two distinct climate states in the absence of a seasonal cycle – one hot and dry, and one  
762 cold and wet; including a seasonal cycle only produces a cold and wet state. While our all-land  
763 simulation is cold and wet near the poles, the absence of surface water redistribution means that  
764 the tropics in our Lakeworld simulation are cold (compared to Aqua or Northland) and dry. Dif-  
765 ferences between our results and those of Kalidindi et al. (2018) arise from the addition of clouds,  
766 zero obliquity, and importantly the resupply of water to low latitudes in their study. We suspect  
767 that without the water recycling mechanism and with a seasonal cycle, Kalidindi et al. (2018)  
768 would also observe low values of soil moisture and precipitation except very close to the poles.

## 769 **5. Conclusions**

770 In this study, we use an idealized climate model to study the climate of Northland, a planet  
771 with a continent covering the NH and an ocean covering the SH, and several related continental  
772 configurations where the NH contains both land and ocean. The physical properties of land on  
773 Earth differ from the ocean in several ways, each of which has an effect on the climate system.  
774 Land has a limited capacity to hold water, a higher albedo, and a smaller heat capacity than oceans,  
775 and evaporation and turbulent energy exchange from the land surface are influenced by properties  
776 of vegetation and soils. By conducting a series of simulations where specific properties of the  
777 land surface are modified, we test the sensitivity of surface climate and atmospheric circulation to  
778 various aspects of the land surface.

779 The climatology of Northland has a seasonal temperature cycle that is greatly amplified over the  
780 land hemisphere, due to the limited heat capacity of the land surface. On the continent, the tropics  
781 are seasonally wet; moisture is brought onto the continent from the ocean by the land-falling  
782 ITCZ, but the soils dry out during NH winter. From 20°N-40°N, there is a desert region. In the  
783 high latitudes, soils are moist year round. There is rain over high latitude land during NH summer;  
784 in contrast, precipitation declines polewards of 45°S in the ocean hemisphere in all seasons. We  
785 show that atmospheric moisture transport forms a swampy region in the high latitudes, both in our  
786 Northland simulations and over a land-only planet.

787 Surprisingly, we find that suppressing terrestrial evaporation over the Northland continent leads  
788 to global-scale cooling, with particularly large cooling of 4.9K over the NH continent – this is in  
789 contrast to previous studies which find reducing terrestrial evaporation warms the land surface.  
790 With all else held equal, decreasing evaporation would lead to warming as the land surface would  
791 have to shed energy through sensible heat or emitted longwave radiation, both of which are a

792 function of surface temperature. However, in our simulations, we find that suppressing terrestrial  
793 evaporation reduces atmospheric water vapor concentrations, and in turn decreases the strength of  
794 the greenhouse effect. The decrease in the greenhouse effect due to reduced water vapor leads to  
795 surface cooling which outweighs any surface warming resulting directly from reduced evaporative  
796 cooling in the Northland continental configuration. Using a series of alternative continental con-  
797 figurations where only part of the NH is covered with land, we demonstrate that there is a trade-off  
798 between the local warming effect of reduced latent heat flux and the global cooling effect of re-  
799 duced atmospheric water vapor. When the NH has two  $90^\circ$  wide continents separated by ocean,  
800 suppressing terrestrial evaporation leads to 1K of warming over land, while a single  $180^\circ$  wide NH  
801 continent leads to weaker warming of 0.7K over land. Three equally spaced  $90^\circ$  wide NH conti-  
802 nents lead to even weaker warming of 0.3K over land, while a single  $270^\circ$  wide continent leads to  
803 cooling of 0.3K over land. The land only experiences warming as a result of suppressed terrestrial  
804 evaporation in regions with soil moisture (i.e. not in the subtropics). Over the oceans, suppress-  
805 ing terrestrial evaporation leads to reduced atmospheric water vapor and decreased downwelling  
806 LW, which reduces sea surface temperatures and ocean evaporation, in turn further reducing at-  
807 mospheric water vapor. We conclude that both globally and over land, the temperature response  
808 to suppressed terrestrial evaporation is not only a function of total land area and the latitudinal  
809 distribution of land, but also of continent size.

810 We find that the ITCZ extends much farther polewards, both over the land and ocean hemi-  
811 spheres, in our Northland simulations compared to an aquaplanet simulation. This is primarily the  
812 result of the difference in surface heat capacity between the land and ocean hemispheres, which  
813 leads to a larger hemispheric imbalance in atmospheric energy in the Northland simulations com-  
814 pared to an aquaplanet.

815 By exploring the climate of Northland, this study provides insight into the role of hemispheric  
816 asymmetries in continental distribution on surface climate and atmospheric circulation, as well as  
817 into energetic constraints on the ITCZ location. We have identified a fundamental trade-off in the  
818 effect of terrestrial evaporation on surface temperatures which warrants further study. Northland  
819 provides an ideal limit for probing fundamental impacts of hemispheric asymmetries and raises  
820 new questions about the role of continental distribution, planetary albedo, and terrestrial evapora-  
821 tion in modulating the climate system.

822 *Data availability statement.* The Isca climate model is publicly available at <https://github.com/ExeClim/Isca>. The data presented in this paper is archived on Dryad, accessible at <https://datadryad.org/stash/dataset/doi:10.6078/D1399Q>.

825 *Acknowledgments.* We wish to thank the organizers of the 2018 Advanced Climate Dy-  
826 namics Course, where this project began (<https://www.uib.no/en/rs/acdc/118773/acdc-2018-hemispheric-asymmetry-climate>). We thank W. R. Boos, A. L. S. Swann, and  
827 W. Kang for their helpful discussions and feedback. We acknowledge postdoctoral funding sup-  
828 port for MML from the James S. McDonnell Foundation Postdoctoral Fellowship in Dynamic and  
829 Multiscale Systems. MP acknowledges funding by the University of Exeter College of Engineer-  
830 ing Mathematics and Physical Sciences, and the UK - China Research and Innovation Partnership  
831 Fund through the Met Office Climate Science for Service Partnership (CSSP) China as part of the  
832 Newton Fund. In addition, MP's gratitude is due to the Rupert Ford Award (administered by the  
833 Royal Meteorological Society) and the University of Exeter College of Engineering Mathematics  
834 and Physical Sciences PhD Mobility Fund who provided the funding for her research visit to the  
835 University of Washington, Seattle, which facilitated collaboration on this project. We thank the  
836 editor and three reviewers for their thoughtful, constructive feedback on this manuscript.  
837

838 **References**

- 839 Abbot, D. S., A. Voigt, D. Li, G. L. Hir, R. T. Pierrehumbert, M. Branson, D. Pollard, and D. D.  
840 B. Koll, 2013: Robust elements of snowball earth atmospheric circulation and oases for life.  
841 *Journal of Geophysical Research: Atmospheres*, **118** (12), 6017–6027.
- 842 Atwood, A. R., A. Donohoe, D. S. Battisti, X. Liu, and F. S. R. Pausata, 2020: Robust  
843 longitudinally-variable responses of the ITCZ to a myriad of climate forcings. *Geophysical*  
844 *Research Letters*, **47** (17), 1–13, doi:10.1029/2020GL088833.
- 845 Bonan, G., 2016: *Ecological Climatology*. 3rd ed., Cambridge University Press, doi:10.1017/  
846 cbo9781107339200.
- 847 Bonan, G. B., 2008: *Ecological Climatology*. Cambridge Univ. Press, Cambridge, UK.
- 848 Bordoni, S., and T. Schneider, 2008: Monsoons as eddy-mediated regime transitions of the tropical  
849 overturning circulation. *Nature Geoscience*, **1** (8), 515–519, doi:10.1038/ngeo248.
- 850 Boynton, W. V., and Coauthors, 2002: Distribution of hydrogen in the near surface of Mars: Evi-  
851 dence for subsurface ice deposits. *Science*, **297** (5578), 81–85, doi:10.1126/science.1073722.
- 852 Broccoli, A. J., K. a. Dahl, and R. J. Stouffer, 2006: Response of the ITCZ to Northern Hemisphere  
853 cooling. *Geophysical Research Letters*, **33** (1), 1–4, doi:10.1029/2005GL024546.
- 854 Budyko, M. I., 1961: The Heat Balance of the Earth's Surface. *Soviet Geography*, **2** (4), 3–13,  
855 doi:10.1080/00385417.1961.10770761.
- 856 Budyko, M. I., 1969: The effect of solar radiation variations on the climate of the Earth. *Tellus*,  
857 **21** (5), 611–619, doi:10.3402/tellusa.v21i5.10109.
- 858 Budyko, M. I., 1974: *Climate and life*. Academic Press, Inc.

859 Byrne, M. P., and P. A. O’Gorman, 2015: The response of precipitation minus evapotranspiration  
860 to climate warming: Why the ”Wet-get-wetter, dry-get-drier” scaling does not hold over land.  
861 *Journal of Climate*, **28 (20)**, 8078–8092, doi:10.1175/JCLI-D-15-0369.1.

862 Canadell, A. J., R. B. Jackson, J. R. Ehleringer, H. A. Mooney, O. E. Sala, and E. Schulze, 1996:  
863 Maximum Rooting Depth of Vegetation Types at the Global Scale. *Oecologia*, **108 (4)**, 583–595.

864 Cess, R. D., and S. D. Goldenberg, 1981: The effect of ocean heat capacity upon global warming  
865 due to increasing atmospheric carbon dioxide. *Journal of Geophysical Research*, **86 (80)**, 498–  
866 502.

867 Charney, J. G., 1975: Dynamics of deserts and drought in the Sahel. *Quarterly Journal of the*  
868 *Royal Meteorological Society*, **101 (428)**, 193–202, doi:10.1002/qj.49710142802.

869 Cheng, L., K. E. Trenberth, J. Fasullo, T. Boyer, J. Abraham, and J. Zhu, 2017: Improved estimates  
870 of ocean heat content from 1960 to 2015. *Science Advances*, **3 (3)**, e1601 545.

871 Chiang, J. C. H., and C. M. Bitz, 2005: Influence of high latitude ice cover on the marine Intertrop-  
872 ical Convergence Zone. *Climate Dynamics*, **25 (5)**, 477–496, doi:10.1007/s00382-005-0040-5.

873 Cho, M. H., A. R. Yang, E. H. Baek, S. M. Kang, S. J. Jeong, J. Y. Kim, and B. M. Kim, 2018:  
874 Vegetation-cloud feedbacks to future vegetation changes in the Arctic regions. *Climate Dynam-*  
875 *ics*, **50 (9-10)**, 3745–3755, doi:10.1007/s00382-017-3840-5.

876 Croll, J., 1870: XII. On ocean-currents. *The London, Edinburgh, and Dublin Philosophical Mag-*  
877 *azine and Journal of Science*, **39 (259)**, 81–106.

878 Davin, E. L., N. de Noblet-Ducoudré, N. de Noblet-Ducoudre, and N. de Noblet-Ducoudré, 2010:  
879 Climatic Impact of Global-Scale Deforestation: Radiative versus Nonradiative Processes. *Jour-*  
880 *nal of Climate*, **23 (1)**, 97–112, doi:10.1175/2009JCLI3102.1.

- 881 Donohoe, A., K. C. Armour, G. H. Roe, D. S. Battisti, and L. Hahn, 2020: The Partitioning of  
882 Meridional Heat Transport from the Last Glacial Maximum to CO<sub>2</sub> Quadrupling in Coupled  
883 Climate Models. *Journal of Climate*, **33** (10), 4141–4165, doi:10.1175/jcli-d-19-0797.1.
- 884 Donohoe, A., and D. S. Battisti, 2011: Atmospheric and surface contributions to planetary albedo.  
885 *Journal of Climate*, **24** (16), 4402–4418, doi:10.1175/2011JCLI3946.1.
- 886 Donohoe, A., J. Marshall, D. Ferreira, and D. Mcgee, 2013: The relationship between ITCZ  
887 location and cross-equatorial atmospheric heat transport: From the seasonal cycle to the Last  
888 Glacial Maximum. *Journal of Climate*, **26** (11), 3597–3618, doi:10.1175/JCLI-D-12-00467.1.
- 889 Eliassen, A., and E. Palm, 1960: On the Transfer of Energy in Stationary Mountain Waves. *Geof-*  
890 *ysiske Publikasjoner*.
- 891 Fasullo, J. T., and K. E. Trenberth, 2008: The Annual Cycle of the Energy Budget. Part II:  
892 Meridional Structures and Poleward Transports. *Journal of Climate*, **21** (10), 2313–2325, doi:  
893 10.1175/2007JCLI1936.1.
- 894 Feldman, W. C., and Coauthors, 2004: Global distribution of near-surface hydrogen on Mars.  
895 *Journal of Geophysical Research E: Planets*, doi:10.1029/2003JE002160.
- 896 Ferrari, R., and D. Ferreira, 2011: What processes drive the ocean heat transport? *Ocean Mod-*  
897 *elling*, doi:10.1016/j.ocemod.2011.02.013.
- 898 Fiorella, R. P., and C. J. Poulsen, 2013: Dehumidification over tropical continents reduces climate  
899 sensitivity and inhibits snowball earth initiation. *Journal of Climate*, **26** (23), 9677–9695.
- 900 Forget, G., and D. Ferreira, 2019: Global ocean heat transport dominated by heat export from the  
901 tropical Pacific. *Nature Geoscience*, doi:10.1038/s41561-019-0333-7.



902 Geen, R., S. Bordoni, D. S. Battisti, and K. Hui, 2020: Monsoons, ITCZs and the Concept of the  
903 Global Monsoon. *Reviews of Geophysics*, 1–45, doi:10.1029/2020rg000700.

904 Geen, R., F. H. Lambert, and G. K. Vallis, 2018: Regime Change Behavior during Asian Monsoon  
905 Onset. *Journal of Climate*, **31** (8), 3327–3348, doi: 10.1175/JCLI-D-17-0118.1.

906 Harris, C. R., and Coauthors, 2020: Array programming with NumPy. *Nature*, **585** (7825), 357–  
907 362, doi:10.1038/s41586-020-2649-2.

908 Hartmann, D. L., 1994: *Global physical climatology*, Vol. 56. Academic press.

909 Held, I. M., 2005: The gap between simulation and understanding in climate modeling. *Bulletin*  
910 *of the American Meteorological Society*, **86** (11), 1609–1614.

911 Held, I. M., P. L. Panetta, and R. T. Pierrehumbert, 1985: Stationary external Rossby waves in  
912 vertical shear. 865–883 pp., doi:10.1175/1520-0469(1985)042<0865:SERWIV>2.0.CO;2.

913 Hoffman, P. F., A. J. Kaufman, G. P. Halverson, and D. P. Schrag, 1998: A Neoproterozoic Snow-  
914 ball Earth. *Science*, **281** (5381), 1342–1346, doi:10.1126/science.281.5381.1342.

915 Hoffman, P. F., and Coauthors, 2017: Snowball Earth climate dynamics and Cryogenian geology-  
916 geobiology. *Science Advances*, **3** (11), doi:10.1126/sciadv.1600983.

917 Hoyer, S., and J. Hamman, 2017: xarray: N-D labeled arrays and datasets in Python. *Journal of*  
918 *Open Research Software*, **5** (1), doi:10.5334/jors.148.

919 Jeevanjee, N., P. Hassanzadeh, S. Hill, and A. Sheshadri, 2017: A perspective on climate model  
920 hierarchies. *Journal of Advances in Modeling Earth Systems*, **9** (4), 1760–1771, doi:10.1002/  
921 2017MS001038.

- 922 Jin, Z., T. P. Charlock, W. L. Smith, and K. Rutledge, 2004: A parameterization of ocean surface  
923 albedo. *Geophysical Research Letters*, **31** (22), 1–4, doi:10.1029/2004GL021180.
- 924 Kalidindi, S., C. H. Reick, T. Raddatz, and M. Claussen, 2018: Two drastically different  
925 climate states on an Earth-like terra-planet. *Earth System Dynamics*, **9** (2), 739–756, doi:  
926 10.5194/esd-9-739-2018.
- 927 Kang, S. M., 2020: Extratropical Influence on the Tropical Rainfall Distribution. **1**, 24–36.
- 928 Kang, S. M., I. M. Held, D. M. W. Frierson, and M. Zhao, 2008: The Response of the ITCZ  
929 to Extratropical Thermal Forcing: Idealized Slab-Ocean Experiments with a GCM. *Journal of*  
930 *Climate*, **21** (14), 3521–3532, doi:10.1175/2007JCLI2146.1.
- 931 Kim, J. E., M. M. Laguë, and A. L. S. Swann, 2020: Evaporative Resistance is of Equal Importance  
932 as Surface Albedo in High-Latitude Surface Temperatures Due to Cloud Feedbacks. 1–10, doi:  
933 10.1029/2019GL085663.
- 934 Kirschvink, J. L., 1992: Late Proterozoic low-latitude global glaciation: the snowball Earth. *The*  
935 *Proterozoic Biosphere*, **52**, 51–52, doi:10.1038/scientificamerican0100-68.
- 936 Kooperman, G. J., Y. Chen, F. M. Hoffman, C. D. Koven, K. Lindsay, M. S. Pritchard, A. L. S.  
937 Swann, and J. T. Randerson, 2018: Forest response to rising CO<sub>2</sub> drives zonally asymmetric  
938 rainfall change over tropical land. *Nature Climate Change*, **8**, doi: 10.1038/s41558-018-0144-7.
- 939 Kuhlbrodt, T., and J. Gregory, 2012: Ocean heat uptake and its consequences for the magnitude of  
940 sea level rise and climate change. *Geophysical Research Letters*, **39** (18).
- 941 Kump, L. R., J. F. Kasting, R. G. Crane, and others, 2004: *The Earth System*, Vol. 432. Pearson  
942 Prentice Hall Upper Saddle River, NJ.

- 943 Laguë, M. M., G. B. Bonan, and A. L. S. Swann, 2019: Separating the Impact of Individual  
944 Land Surface Properties on the Terrestrial Surface Energy Budget in both the Coupled and  
945 Uncoupled Land–Atmosphere System. *Journal of Climate*, **32 (18)**, 5725–5744, doi:10.1175/  
946 jcli-d-18-0812.1.
- 947 Laguë, M. M., and A. L. Swann, 2016: Progressive midlatitude afforestation: Impacts on clouds,  
948 global energy transport, and precipitation. *Journal of Climate*, **29 (15)**, 5561–5573, doi:10.1175/  
949 jcli-d-15-0748.1.
- 950 Levins, R., 1966: The Strategy of Model Building in Population Biology. *American Scientist*,  
951 **5 (41)**, 420–431.
- 952 Loft, G., 1918: The Gulf Stream and the North Atlantic Drift. *Journal of Geography*, **17 (1)**, 8–17,  
953 doi:10.1080/00221341808984367.
- 954 Maher, P., and Coauthors, 2019: Model Hierarchies for Understanding Atmospheric Circulation.  
955 doi:10.1029/2018RG000607.
- 956 Manabe, S., 1969: Climate and the Ocean Circulation. *Monthly Weather Review*, **97 (11)**, 739–  
957 774, doi:10.1175/1520-0493(1969)097<0739:CATOC>2.3.CO;2.
- 958 Manabe, S., R. J. Stouffer, M. J. Spelman, and K. Bryan, 1991: Transient responses of a cou-  
959 pled ocean–atmosphere model to gradual changes of atmospheric CO<sub>2</sub>. Part I. Annual mean  
960 response. *Journal of Climate*, **4 (8)**, 785–818.
- 961 Manabe, S., and T. B. Terpstra, 1974: The effect of mountains on the general circulation of the  
962 Atmosphere. 3 pp.

963 Maroon, E. A., D. M. Frierson, S. M. Kang, and J. Scheff, 2016: The precipitation response  
964 to an idealized subtropical continent. *Journal of Climate*, **29** (12), 4543–4564, doi:10.1175/  
965 JCLI-D-15-0616.1.

966 Marshall, D. P., and L. Zanna, 2014: A conceptual model of ocean heat uptake under climate  
967 change. *Journal of Climate*, **27** (22), 8444–8465.

968 Marshall, J., and R. A. Plumb, 2008: *Atmosphere, ocean, and climate dynamics: an introductory*  
969 *text*, Vol. 93. Elsevier Academic Press.

970 McFarlane, N. A., 1987: The Effect of Orographically Excited Gravity Wave Drag on the Gen-  
971 eral Circulation of the Lower Stratosphere and Troposphere. 1775–1800 pp., doi:10.1175/  
972 1520-0469(1987)044<1775:teooeg>2.0.co;2.

973 McMullin, E., 1985: Galilean idealization. *Studies in History and Philosophy of Science Part A*,  
974 **16** (3), 247–273.

975 Milly, P. C. D., and a. B. Shmakin, 2002: Global Modeling of Land Water and Energy Balances.  
976 Part I: The Land Dynamics (LaD) Model. *Journal of Hydrometeorology*, **3** (3), 283–299, doi:  
977 10.1175/1525-7541(2002)003<0283:GMOLWA>2.0.CO;2.

978 Nilsson, J., P. L. Langen, D. Ferreira, and J. Marshall, 2013: Ocean basin geometry and the  
979 salinification of the Atlantic Ocean. *Journal of Climate*, doi:10.1175/JCLI-D-12-00358.1.

980 North, G. R., J. G. Mengel, and D. A. Short, 1983: Simple energy balance model resolving the  
981 seasons and the continents: Application to the astronomical theory of the ice ages. *Journal of*  
982 *Geophysical Research*, **88** (C11), 6576–6586, doi:10.1029/JC088iC11p06576.

983 Oke, T. R., 1987: *Boundary layer climates, Second edition*. doi:10.1017/CBO9781107415324.  
984 004.

985 Payne, R. E., 1972: Albedo of the Sea Surface. 959–970 pp., doi:10.1175/1520-0469(1972)  
986 029(0959:aotss)2.0.co;2.

987 Pietschnig, M., F. H. Lambert, M. Saint-Lu, and G. K. Vallis, 2019: The Presence of Africa and  
988 Limited Soil Moisture Contribute to Future Drying of South America. *Geophysical Research  
989 Letters*, **46 (21)**, 12 445–12 453, doi:10.1029/2019GL084441.

990 Queney, P., 1948: The Problem of Air Flow Over Mountains: A Summary of Theoretical Studies.  
991 *Bulletin of the American Meteorological Society*, **29 (1)**, 16–26, doi:10.1175/1520-0477-29.1.  
992 16.

993 Richardson, P. L., 1980: Benjamin Franklin and Timothy Folger’s First Printed Chart of the Gulf  
994 Stream. *Science*, **207 (4431)**, 643–645.

995 Rose, B. E. J., K. C. Armour, D. S. Battisti, N. Feldl, and D. D. B. Koll, 2014: The dependence of  
996 transient climate sensitivity and radiative feedbacks on the spatial pattern of ocean heat uptake.  
997 *Geophysical Research Letters*, **41 (3)**, 1071–1078.

998 Sellers, P. J., and Coauthors, 1996: Comparison of radiative and physiological effects of dou-  
999 bled atmospheric CO<sub>2</sub> on climate. *SCIENCE-NEW YORK THEN WASHINGTON-*, **271 (5254)**,  
1000 1402–1405, doi:10.1126/science.271.5254.1402.

1001 Sellers, W. D., 1969: Global Climatic Model Based on the Energy Balance of the Earth-  
1002 Atmosphere System. *Journal of Applied Meteorology*, **8 (3)**, 392–400.

1003 Shukla, J., and Y. Mintz, 1982: Influence of Land-Surface Evapotranspiration on the Earth’s Cli-  
1004 mate. *Science*, **215 (4539)**, 1498–1501.

- 1005 Sikma, M., and J. Vilà-Guerau de Arellano, 2019: Substantial Reductions in Cloud Cover and  
1006 Moisture Transport by Dynamic Plant Responses. *Geophysical Research Letters*, **46** (3), 1870–  
1007 1878, doi:10.1029/2018GL081236.
- 1008 Stocker, T. F., and Coauthors, 2013: Climate change 2013 the physical science basis: Working  
1009 Group I contribution to the fifth assessment report of the Intergovernmental Panel on Climate  
1010 Change. *Contribution of Working Group I to the Fifth Assessment Report of the Intergovern-  
1011 mental Panel on Climate Change.*, **9781107057**, 1–1535, doi:10.1017/CBO9781107415324.
- 1012 Stouffer, R. J., S. Manabe, and K. Bryan, 1989: Interhemispheric asymmetry in climate response  
1013 to a gradual increase of atmospheric CO<sub>2</sub>. *Nature*, **342** (6250), 660–662.
- 1014 Sud, Y. C., J. Shukla, and Y. Mintz, 1988: Influence of Land Surface Roughness on Atmospheric  
1015 Circulation and Precipitation: A Sensitivity Study with a General Circulation Model. 1036–  
1016 1054 pp., doi:10.1175/1520-0450(1988)027<1036:iolsro>2.0.co;2.
- 1017 Sutton, R. T., B. Dong, and J. M. Gregory, 2007: Land/sea warming ratio in response to climate  
1018 change: IPCC AR4 model results and comparison with observations. *Geophysical Research  
1019 Letters*, **34** (2), 2–6, doi:10.1029/2006GL028164.
- 1020 Swann, A. L. S., I. Y. Fung, and J. C. H. Chiang, 2012: Mid-latitude afforestation shifts general  
1021 circulation and tropical precipitation. *Proceedings of the National Academy of Sciences*, **109** (3),  
1022 712–716, doi:10.1073/pnas.1116706108.
- 1023 Thomson, S. I., and G. K. Vallis, 2019: Hierarchical Modeling of Solar System Planets with Isca.  
1024 *Atmosphere*, **10** (12), 803, doi: 10.3390/atmos10120803.
- 1025 Trenberth, K. E., and J. M. Caron, 2001: Estimates of meridional atmosphere and ocean heat  
1026 transports. *Journal of Climate*, **14** (16), 3433–3443.

- 1027 Vallis, G. K., and Coauthors, 2018: Isca, v1.0: A framework for the global modelling of the  
1028 atmospheres of Earth and other planets at varying levels of complexity. *Geoscientific Model*  
1029 *Development*, **11** (3), 843–859, doi:10.5194/gmd-11-843-2018.
- 1030 Voigt, A., 2013: The dynamics of the Snowball Earth Hadley circulation for off-equatorial  
1031 and seasonally varying insolation. *Earth System Dynamics*, **4** (2), 425–438, doi:10.5194/  
1032 esd-4-425-2013.
- 1033 Voigt, A., D. Abbot, R. Pierrehumbert, and J. Marotzke, 2011: Initiation of a marinoan snowball  
1034 earth in a state-of-the-art atmosphere-ocean general circulation model. *Climate of the Past*, **7**,  
1035 249–263.
- 1036 Voigt, A., S. Bony, J. L. Dufresne, and B. Stevens, 2014: The radiative impact of clouds on the  
1037 shift of the Intertropical Convergence Zone. *Geophysical Research Letters*, **41** (12), 4308–4315,  
1038 doi:10.1002/2014GL060354.
- 1039 Voigt, A., I. M. Held, and J. Marotzke, 2012: Hadley cell dynamics in a virtually dry snow-  
1040 ball Earth atmosphere. *Journal of the Atmospheric Sciences*, **69** (1), 116–128, doi:10.1175/  
1041 JAS-D-11-083.1.
- 1042 Voigt, A., and Coauthors, 2016: The tropical rain belts with an annual cycle and a continent model  
1043 intercomparison project: TRACMIP. *Journal of Advances in Modeling Earth Systems*, **8** (4),  
1044 1868–1891, doi:10.1002/2016MS000748.
- 1045 Wallace, J. M., Y. Zhang, and J. A. Renwick, 1995: Dynamic Contribution to Hemispheric Mean  
1046 Temperature Trends. *Science*, **270** (5237), 780–783.

- 1047 Wei, H.-H., and S. Bordoni, 2018: Energetic Constraints on the ITCZ Position in Idealized Simu-  
1048 lations With a Seasonal Cycle. *Journal of Advances in Modeling Earth Systems*, **10** (7), 1708–  
1049 1725, doi: 10.1029/2018MS001313.
- 1050 Wiscombe, W., and S. Warren, 1980: A Model for Spectral Albedo I: Pure Snow. 2712–2733 pp.
- 1051 Wordsworth, R. D., 2016: The Climate of Early Mars. *Annual Review of Earth and Planetary*  
1052 *Sciences*, **44** (1), 381–408, doi:10.1146/annurev-earth-060115-012355.
- 1053 Worsley, T. R., and D. L. Kidder, 1991: First-order coupling of paleogeography and CO<sub>2</sub>, with  
1054 global surface temperature and its latitudinal contrast. *Geology*, **19** (12), 1161–1164, doi:10.  
1055 1130/0091-7613(1991)019<1161:FOCOPA>2.3.CO;2.
- 1056 Yoshimori, M., and A. J. Broccoli, 2008: Equilibrium Response of an Atmosphere-Mixed Layer  
1057 Ocean Model to Different Radiative Forcing Agents: Global and Zonal Mean Response. *Journal*  
1058 *of Climate*, **21** (17), 4399–4423, doi:10.1175/2008JCLI2172.1.
- 1059 Zarakas, C. M., A. L. Swann, M. M. Laguë, K. C. Armour, and J. T. Randerson, 2020: Plant  
1060 Physiology Increases the Magnitude and Spread of the Transient Climate Response to CO<sub>2</sub> in  
1061 CMIP6 Earth System Models. *Journal of Climate*, 1–44, doi:10.1175/jcli-d-20-0078.1.
- 1062 Zelinka, M. D., D. A. Randall, M. J. Webb, and S. A. Klein, 2017: Clearing clouds of uncertainty.  
1063 *Nature Climate Change*, **7** (10), 674–678, doi:10.1038/nclimate3402.



1064 **LIST OF TABLES**

1065 **Table 1.** List of the idealized-continent Isca simulations used in this study, along with  
1066 the land surface property values for each experiment. . . . . 49

TABLE 1. List of the idealized-continent Isca simulations used in this study, along with the land surface

property values for each experiment.

Experiment name	Description	Land albedo	Bucket depth [m H <sub>2</sub> O]	Initial water in bucket [m H <sub>2</sub> O]
<b>NorthlandBright</b>	Northern hemisphere continent with an albedo brighter than the ocean.	0.325	0.15	0.1
<b>NorthlandDark</b>	Northern hemisphere continent with the same albedo as the ocean.	0.25	0.15	0.1
<b>NorthlandEmpty</b>	Like NorthlandBright, but initialized with no water on the land surface.	0.325	0.15	0
<b>NorthlandDry</b>	Like NorthlandBright, but with a very small capacity for the land to hold water.	0.325	0.00001	0
<b>Lakeworld</b>	All-land planet with bucket hydrology modified to allow lakes to form.	0.325	0.15	0.1
<b>NorthWestLand</b>	Single 180°-longitude wide continent from 0-90°N, covering 25% of the planet's surface. Land surface properties same as NorthlandBright.	0.325	0.15	0.1
<b>NorthWestLandDry</b>	Same as NorthWestLand, but with the same land surface properties as as NorthlandDry.	0.325	0.00001	0
<b>ThreeQuarterLand</b>	Single 270°-longitude wide continent from 0-90°N, covering 75% of the NH (¾ of the total planetary surface). Land surface properties same as NorthlandBright.	0.325	0.15	0.1
<b>ThreeQuarterLandDry</b>	Same as ThreeQuarterLand, but with the same land surface properties as as NorthlandDry.	0.325	0.00001	0
<b>TwoPatchLand</b>	Two equally-spaced 90°-longitude wide continents from 0-90°N, covering a combined total 25% of the planet's surface. Land surface properties same as NorthlandBright.	0.325	0.15	0.1
<b>TwoPatchLandDry</b>	Same as TwoPatchLand, but with the land surface properties the same as NorthlandDry.	0.325	0.00001	0
<b>ThreePatchLand</b>	Three equally-spaced 90°-longitude wide continents from 0-90°N, covering a combined total 75% of the NH. Land surface properties same as NorthlandBright.	0.325	0.15	0.1
<b>ThreePatchLandDry</b>	Same as ThreePatchLand, but with the land surface properties the same as NorthlandDry.	0.325	0.00001	0
<b>Aqua</b>	Aquaplanet simulation with 20m mixed layer (no land)	–	–	–

## LIST OF FIGURES

1069		
1070	<b>Fig. 1.</b>	Maps of the continental distributions used in this study. Grey areas indicate land, while white areas indicate ocean. . . . . 52
1071		
1072	<b>Fig. 2.</b>	Zonal mean temperature (a,c) and precipitation (b,d). The NorthlandBright simulation is shown in (a) & (b) (solid lines). The anomalies for NorthlandDark - NorthlandBright (dashed lines) and NorthlandDry - NorthlandBright (dotted lines) are shown in (c) & (d). In a-d, black lines indicate annual mean values, while blue (red) show values for December/January/February (June/July/August) in (a,c) and cyan (magenta) show values for February/March/April (August/September/October) in (b,d). Shading in a-d indicates $\pm 1$ standard deviation. Panels (e,f) show the annual mean change in zonal mean relative humidity (shading) and temperature (contours) for (e) NorthlandDark-NorthlandBright and (f) NorthlandDry-NorthlandBright. Temperature contours (red/blue lines in e-f) are spaced at 1K, with red values $> 0$ and blue values $< 0$ . Only humidity values in (e,f) which differ significantly ( $p < 0.05$ using a student's t-test) are shown. . . . . 53
1073		
1074		
1075		
1076		
1077		
1078		
1079		
1080		
1081		
1082		
1083	<b>Fig. 3.</b>	Zonal mean seasonal cycle of (a) precipitation, (b) evaporation, and (c) precipitation-evaporation (P-E) for the spun-up NorthlandBright simulation; the equator/continental boundary is marked by the solid black line. Zonal mean terrestrial water storage over the first 6 simulation years for (d) NorthlandBright and (e) NorthlandEmpty. Zonal mean terrestrial water storage for (f) the full 80 year simulation of Lakeworld (note the non-linear color bar). Cyan contour in (f) at 150mm shows the bucket capacity (i.e. fully saturated soil moisture). . . . . 54
1084		
1085		
1086		
1087		
1088		
1089		
1090	<b>Fig. 4.</b>	Seasonal cycle of zonal mean precipitation from 40°S to 40°N in (a) NorthlandBright, (b) NorthlandDark, (c) NorthlandDry, and (d) Aqua. . . . . 55
1091		
1092	<b>Fig. 5.</b>	Change in the zonal mean surface energy budget for NorthlandDry - NorthlandBright over the course of the year. The change in downwards $LW$ is shown in (a) while the change in net SFC $SW$ is shown in (b). $LW$ emitted by the surface is shown in (c), while (d) and (e) show sensible and latent heat, respectively. (f) shows the change in net surface energy uptake ( $E_{in} = SW^{\downarrow} - SW^{\uparrow} + LW^{\downarrow}$ ), where positive values indicate more energy into the surface; in the annual mean this would be balanced by $E_{out} = LW^{\uparrow} + LH + SH$ . . . . . 56
1093		
1094		
1095		
1096		
1097		
1098	<b>Fig. 6.</b>	Change in the zonal mean TOA energy budget for NorthlandDry - NorthlandBright over the course of the year. The change in net TOA $SW$ is shown in (a) while the change in outgoing longwave radiation is shown in (b). The net TOA energy budget (a-b) is shown in (c). The change in the atmospheric energy source $F_{net} = TOA_{net} - SFC_{net}$ is shown in (d), where positive indicates more energy into the atmosphere. . . . . 57
1099		
1100		
1101		
1102		
1103	<b>Fig. 7.</b>	Annual mean change in surface temperature (left), latent heat flux (center), and percent change in zonal mean specific humidity (right) for suppressing terrestrial evaporation in various continental configurations. Thick black lines show the continental boundary. . . . . 58
1104		
1105		
1106	<b>Fig. 8.</b>	The area-weighted annual mean change in (a) surface temperature and (b) latent heat flux globally (gray), over land only (green), and over the ocean only (blue), for each continental configuration. Small vertical black lines on each bar indicate 1 standard deviation. The magnitude of the temperature/latent heat flux change is noted above or below each bar. The total global land fraction for each simulation is noted along the bottom of each panel. . . . . 59
1107		
1108		
1109		
1110		

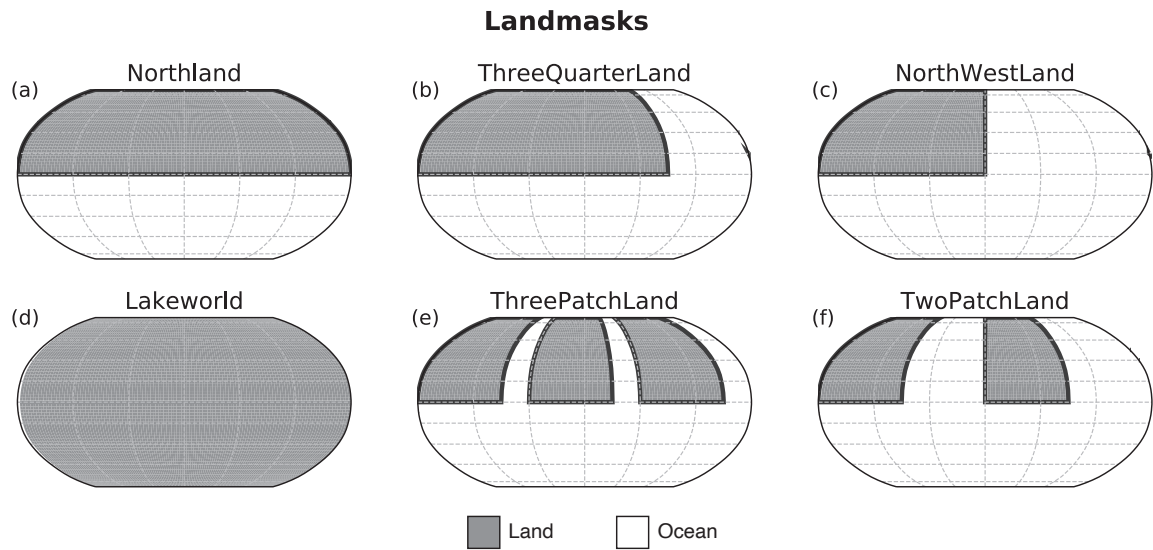
1111 **Fig. 9.** Change in surface temperature (left), change in latent heat flux (center), and percent change  
1112 in zonal mean specific humidity (right) between NorthlandDark and Aqua. The annual mean  
1113 change is shown in a-c, while the zonal-mean seasonal cycle is shown in d-e. . . . . 60

1114 **Fig. 10.** Top: zonal mean percent change in annual mean specific humidity for (a) NorthlandBright -  
1115 Aqua and (b) NorthlandDark - Aqua. Middle: seasonal cycle of the zonal mean change in net  
1116 SW absorbed at the surface for (c) NorthlandBright - Aqua and (d) NorthlandDark - Aqua.  
1117 Bottom: ITCZ latitude calculated as the center of mass of zonal mean precipitation from  
1118 30°S to 30°N for NorthlandBright, NorthlandDark, and Aqua, where each dot represents a  
1119 single month of the year. . . . . 61

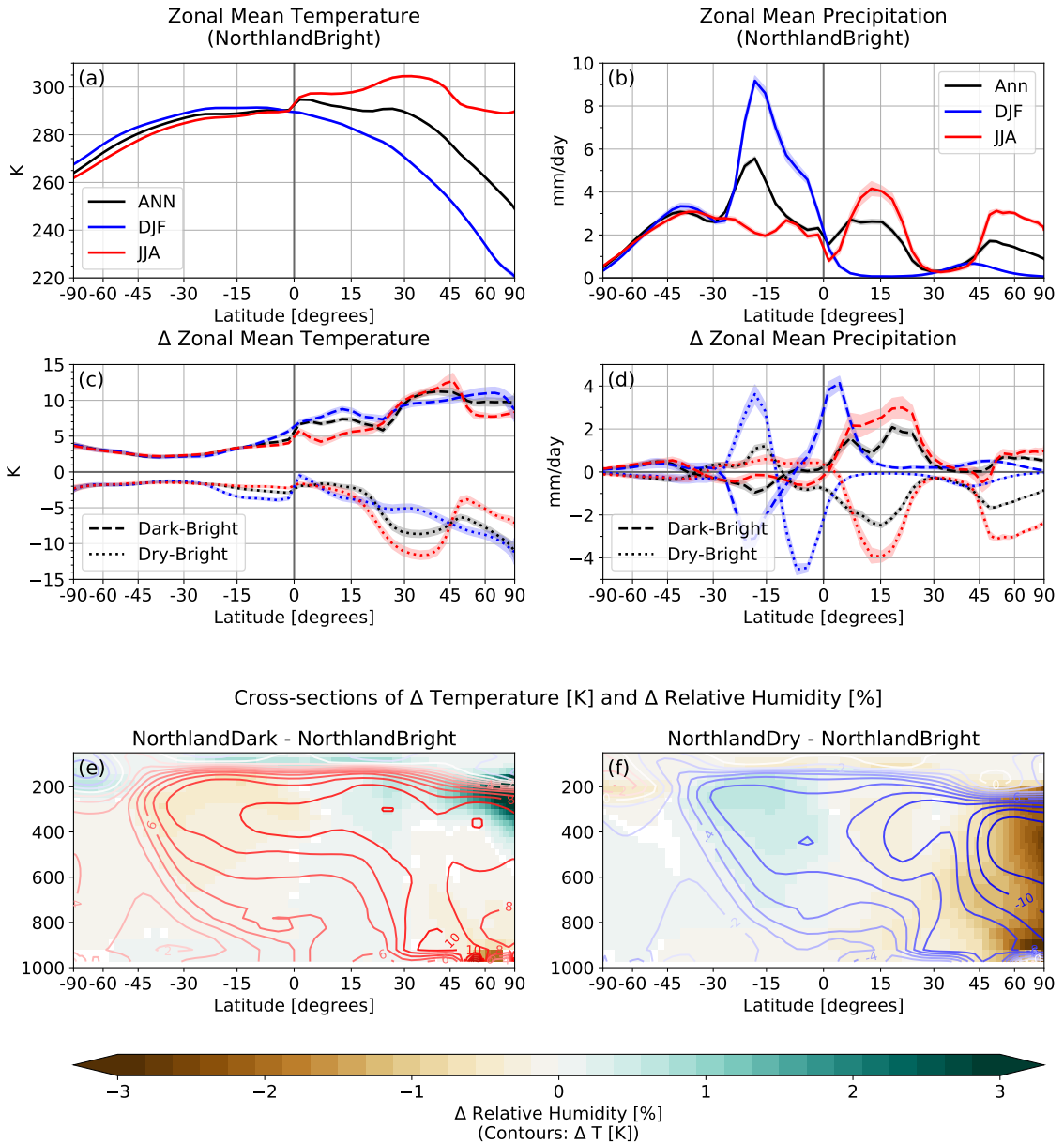
1120 **Fig. 11.** Relationship between the latitude of the ITCZ and the magnitude of cross-equatorial energy  
1121 flux. The latitude of the ITCZ is calculated as the center of mass of precipitation between  
1122 30°S and 30°N; the magnitude of cross-equatorial energy flux is calculated as the magnitude  
1123 of meridional atmospheric energy transport at the equator. Black markers indicate annual  
1124 mean values, while blue, purple, green, and red markers indicate DJF, MAM, JJA, and SON  
1125 averages, respectively. Circles show values for NorthlandBright, x for NorthlandDark, and  
1126 triangles for Aqua. Each individual marker shows the seasonally averaged value for a single  
1127 year of the time series. NorthlandDry is not included in the regression calculations here as  
1128 the ITCZ effectively collapses over the continent. . . . . 62

1129 **Fig. 12.** Zonally averaged net TOA energy flux ( $TOA$ , blue dotted line), net surface energy flux  
1130 ( $SFC$ , green dash-dot line), and the atmospheric column energy source ( $F_{net} = TOA - SFC$ ;  
1131 black solid line) for the annual mean (top row), DJF (middle row) and JJA (bottom row).  
1132 NorthlandBright is shown in the first column, NorthlandDark in the second, NorthlandDry in  
1133 the third, and Aqua in the fourth. The total column integrated cross-equatorial atmospheric  
1134 energy transport (positive northwards) for each season is noted in the lower right of each  
1135 panel. . . . . 63

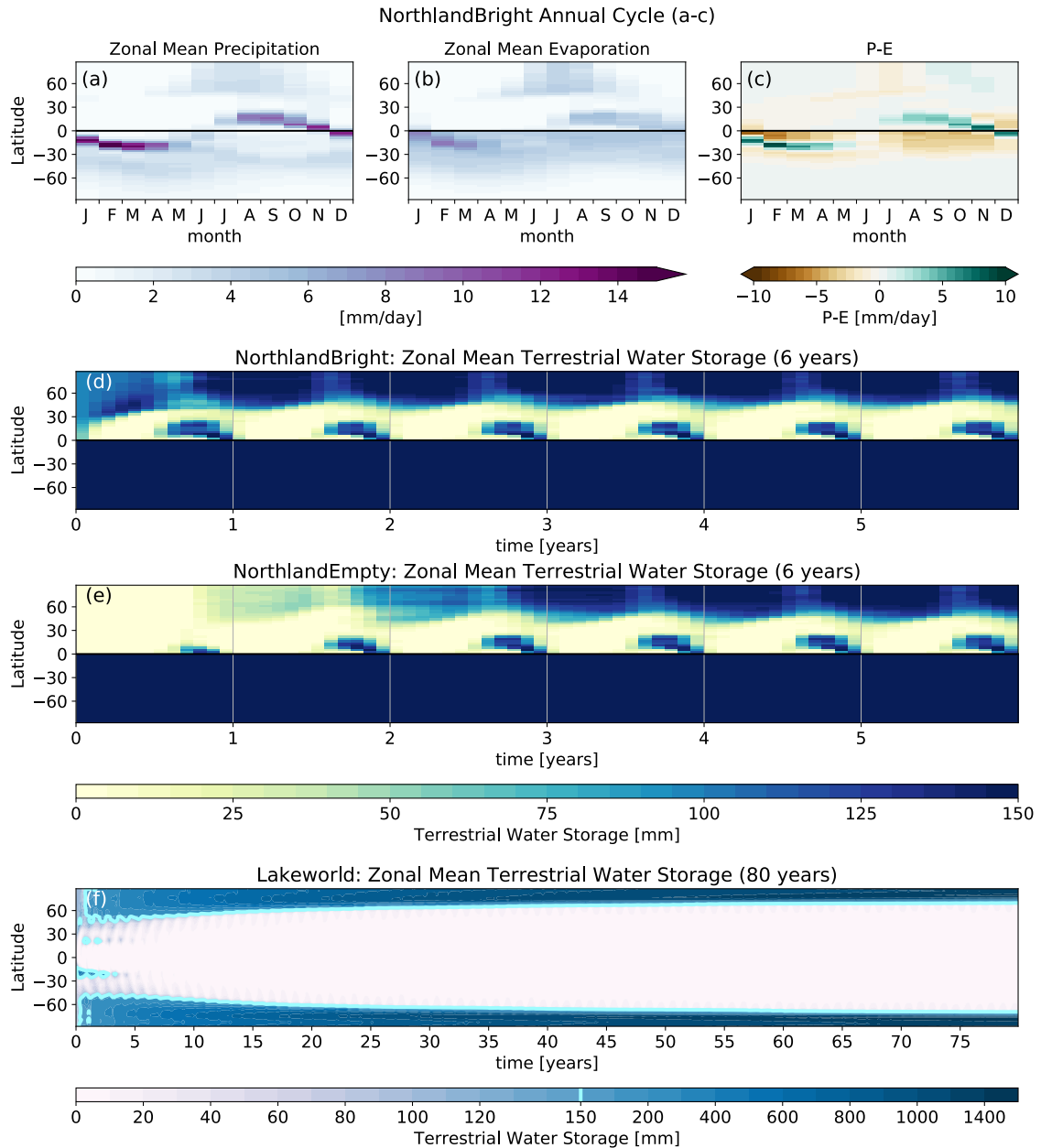
1136 **Fig. 13.** Schematic showing the surface temperature response to suppressed terrestrial evaporation  
1137 for a variety of NH continental configurations. Land area generally increases from left to  
1138 right, though for a given total land area, larger continents sit farther to the right on the curve  
1139 than smaller, more numerous continents. Qualitative locations of suppressing terrestrial  
1140 evaporation on TwoPatchLand, NorthWestLand, ThreePatchLand, ThreeQuarterLand, and  
1141 Northland are shown by the maps of temperature change for each continental configuration,  
1142 with the annual mean change in land surface temperature noted on each map. . . . . 64



1143 FIG. 1. Maps of the continental distributions used in this study. Grey areas indicate land, while white areas  
 1144 indicate ocean.

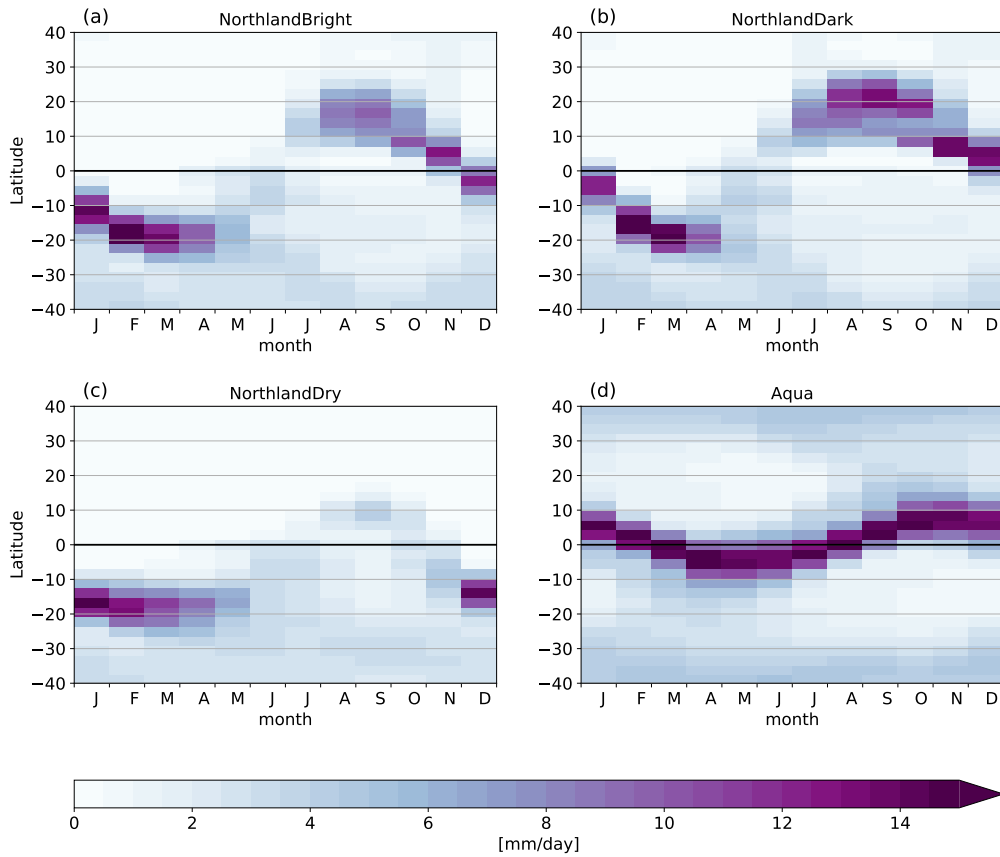


1145 FIG. 2. Zonal mean temperature (a,c) and precipitation (b,d). The NorthlandBright simulation is shown in  
 1146 (a) & (b) (solid lines). The anomalies for NorthlandDark - NorthlandBright (dashed lines) and NorthlandDry -  
 1147 NorthlandBright (dotted lines) are shown in (c) & (d). In a-d, black lines indicate annual mean values, while blue  
 1148 (red) show values for December/January/February (June/July/August) in (a,c) and cyan (magenta) show values  
 1149 for February/March/April (August/September/October) in (b,d). Shading in a-d indicates  $\pm 1$  standard deviation.  
 1150 Panels (e,f) show the annual mean change in zonal mean relative humidity (shading) and temperature (contours)  
 1151 for (e) NorthlandDark-NorthlandBright and (f) NorthlandDry-NorthlandBright. Temperature contours (red/blue  
 1152 lines in e-f) are spaced at 1K, with red values  $> 0$  and blue values  $< 0$ . Only humidity values in (e,f) which  
 1153 differ significantly ( $p < 0.05$  using a student's t-test) are shown.



1154 FIG. 3. Zonal mean seasonal cycle of (a) precipitation, (b) evaporation, and (c) precipitation-evaporation (P-  
 1155 E) for the spun-up NorthlandBright simulation; the equator/continental boundary is marked by the solid black  
 1156 line. Zonal mean terrestrial water storage over the first 6 simulation years for (d) NorthlandBright and (e)  
 1157 NorthlandEmpty. Zonal mean terrestrial water storage for (f) the full 80 year simulation of Lakeworld (note  
 1158 the non-linear color bar). Cyan contour in (f) at 150mm shows the bucket capacity (i.e. fully saturated soil  
 1159 moisture).

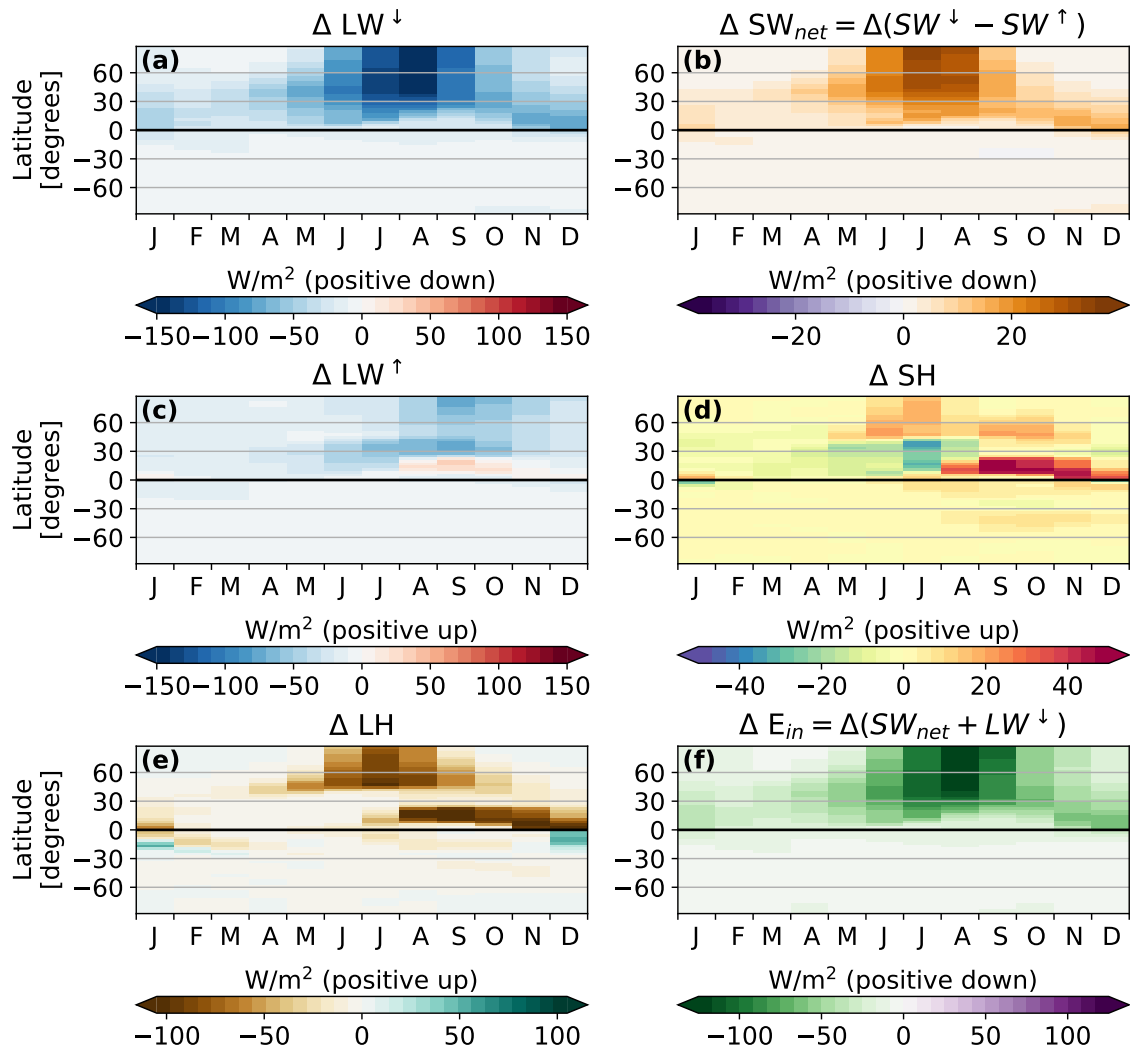
Seasonal Cycle of Zonal Mean Precipitation [mm/day]



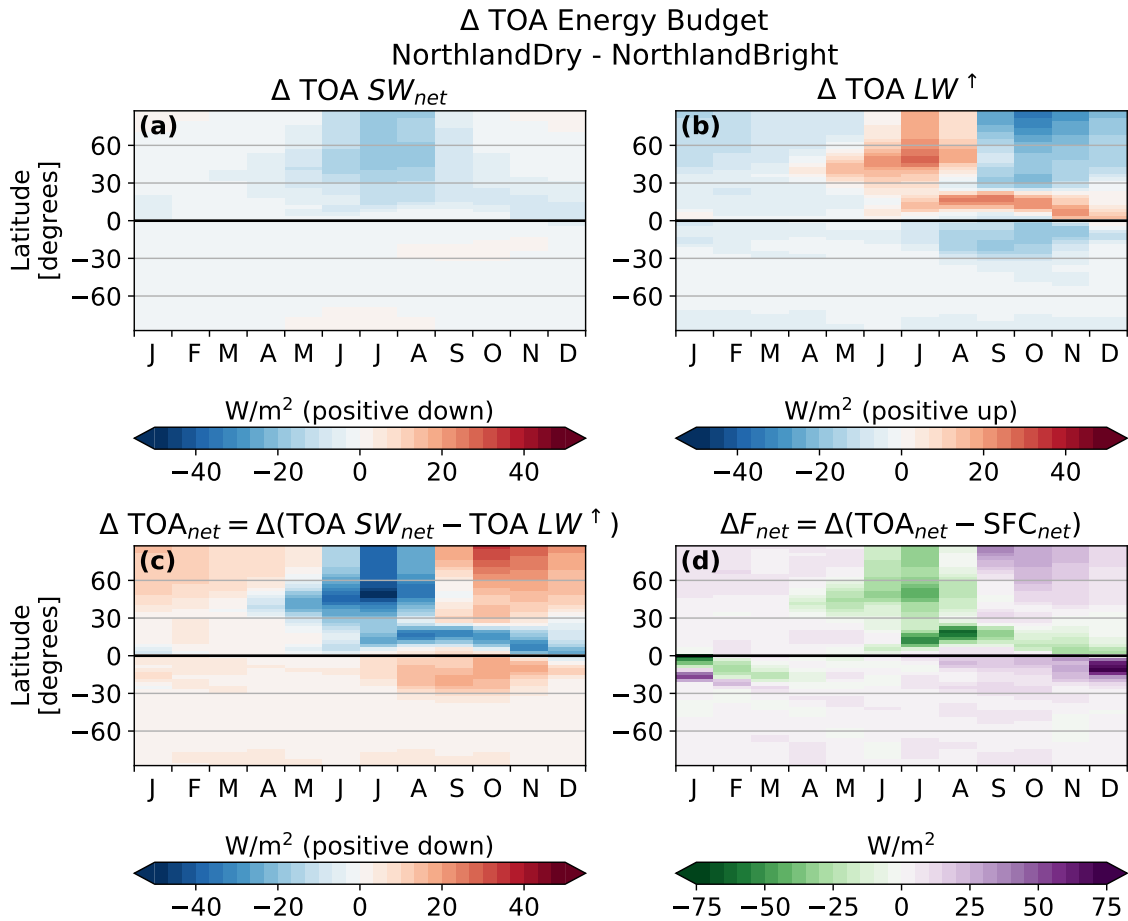
1160 FIG. 4. Seasonal cycle of zonal mean precipitation from 40°S to 40°N in (a) NorthlandBright, (b) Northland-  
1161 Dark, (c) NorthlandDry, and (d) Aqua.



$\Delta$  SFC Energy Budget  
NorthlandDry - NorthlandBright

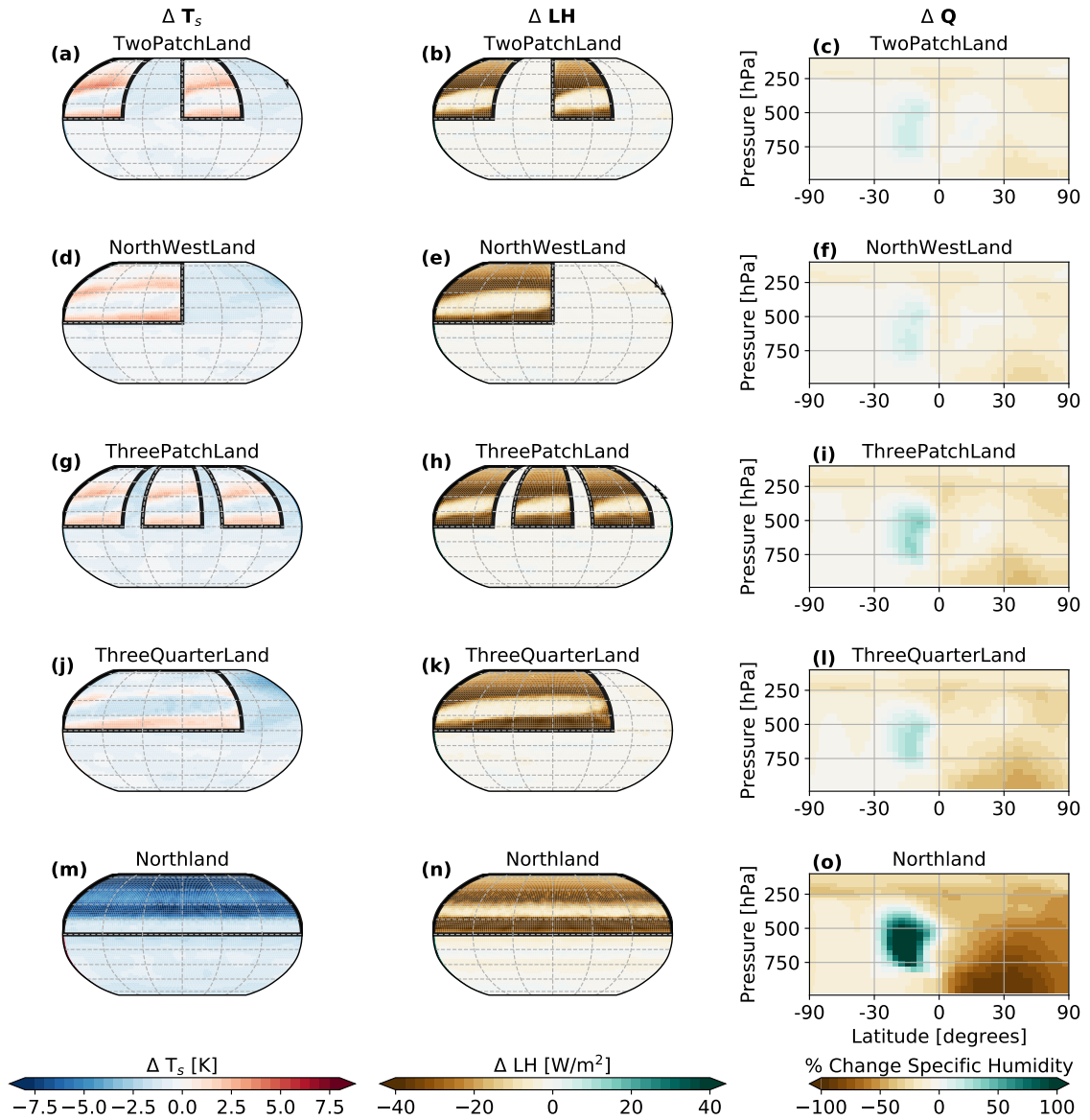


1162 FIG. 5. Change in the zonal mean surface energy budget for NorthlandDry - NorthlandBright over the course  
 1163 of the year. The change in downwards  $LW$  is shown in (a) while the change in net SFC  $SW$  is shown in (b).  $LW$   
 1164 emitted by the surface is shown in (c), while (d) and (e) show sensible and latent heat, respectively. (f) shows the  
 1165 change in net surface energy uptake ( $E_{in} = SW^\downarrow - SW^\uparrow + LW^\downarrow$ ), where positive values indicate more energy into  
 1166 the surface; in the annual mean this would be balanced by  $E_{out} = LW^\uparrow + LH + SH$ .

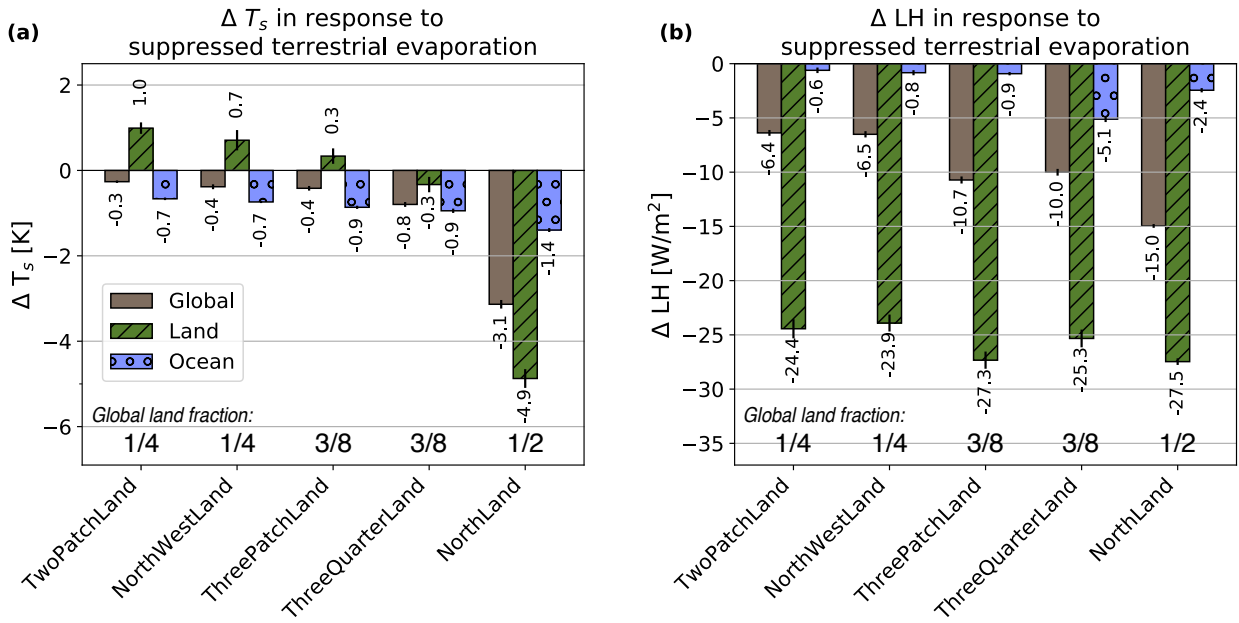


1167 FIG. 6. Change in the zonal mean TOA energy budget for NorthlandDry - NorthlandBright over the course  
 1168 of the year. The change in net TOA  $SW$  is shown in (a) while the change in outgoing longwave radiation is  
 1169 shown in (b). The net TOA energy budget (a-b) is shown in (c). The change in the atmospheric energy source  
 1170  $F_{net} = TOA_{net} - SFC_{net}$  is shown in (d), where positive indicates more energy into the atmosphere.

**Effect of Suppressing Terrestrial Evaporation on  
Surface Temperature and Specific Humidity**

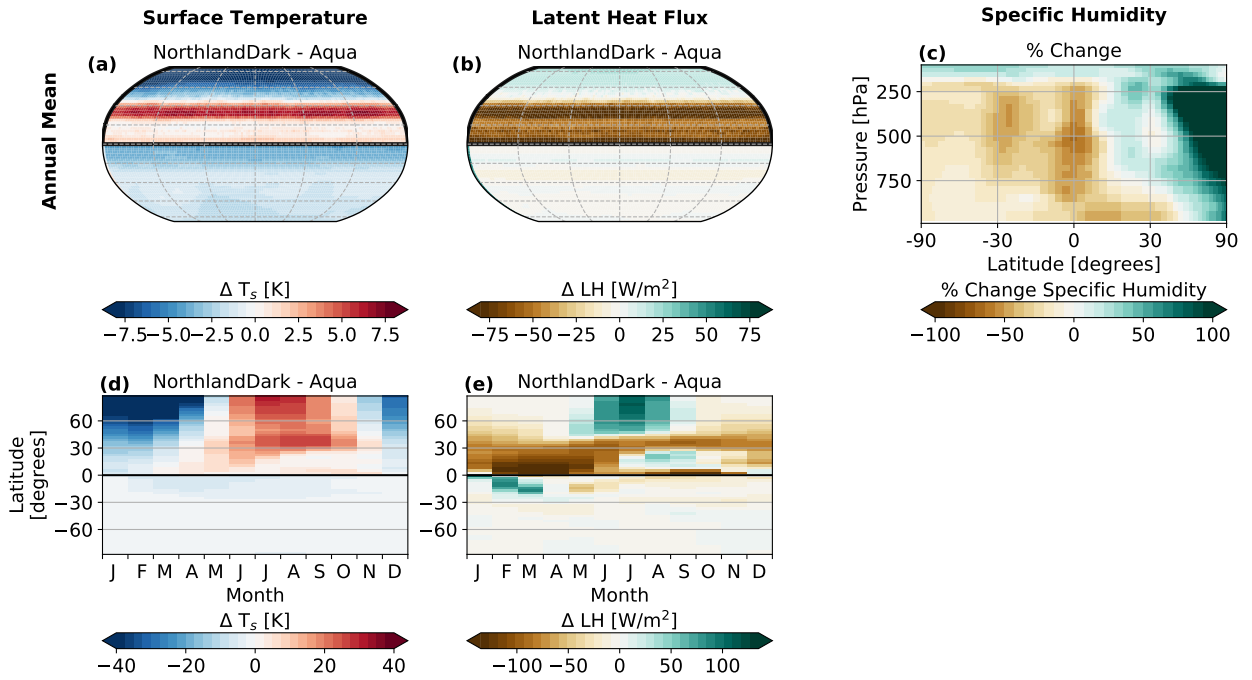


1171 FIG. 7. Annual mean change in surface temperature (left), latent heat flux (center), and percent change in  
 1172 zonal mean specific humidity (right) for suppressing terrestrial evaporation in various continental configurations.  
 1173 Thick black lines show the continental boundary.

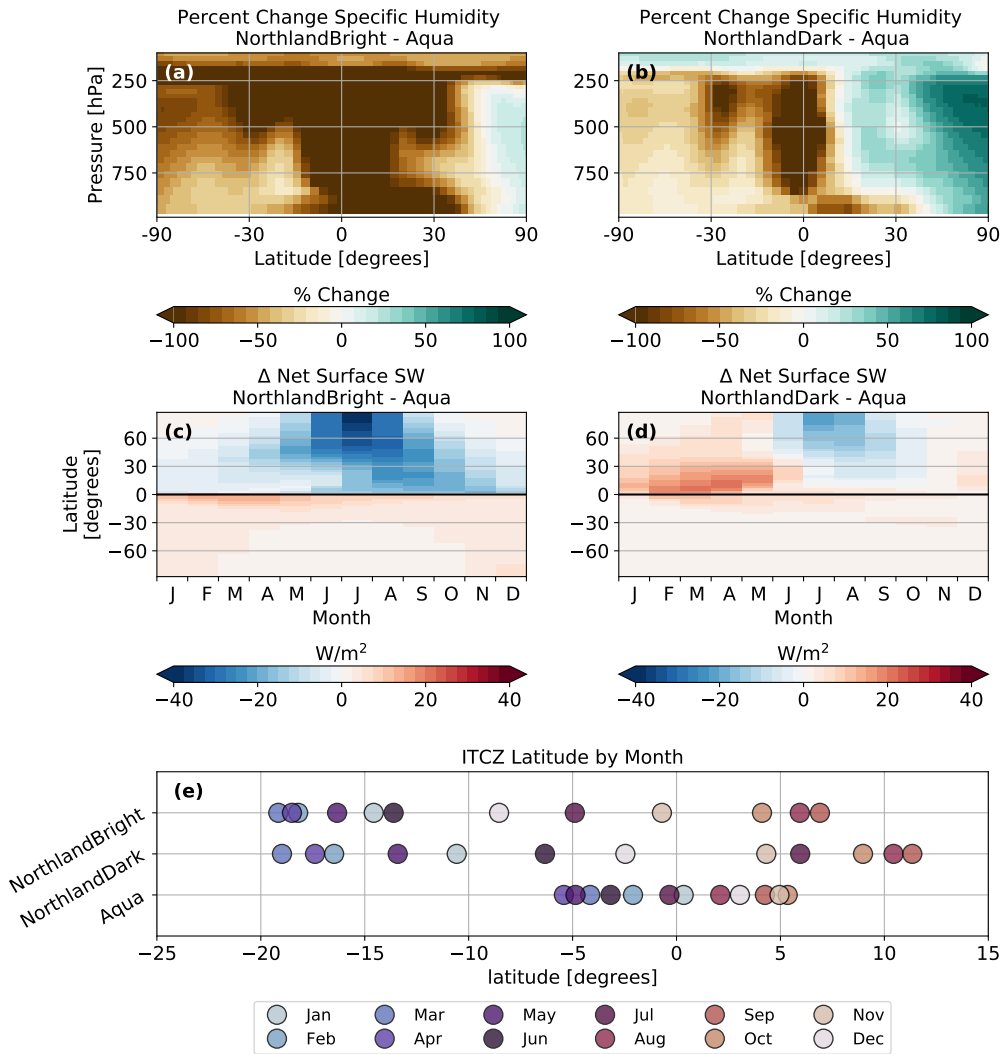


1174 FIG. 8. The area-weighted annual mean change in (a) surface temperature and (b) latent heat flux globally  
 1175 (gray), over land only (green), and over the ocean only (blue), for each continental configuration. Small vertical  
 1176 black lines on each bar indicate 1 standard deviation. The magnitude of the temperature/latent heat flux change  
 1177 is noted above or below each bar. The total global land fraction for each simulation is noted along the bottom of  
 1178 each panel.

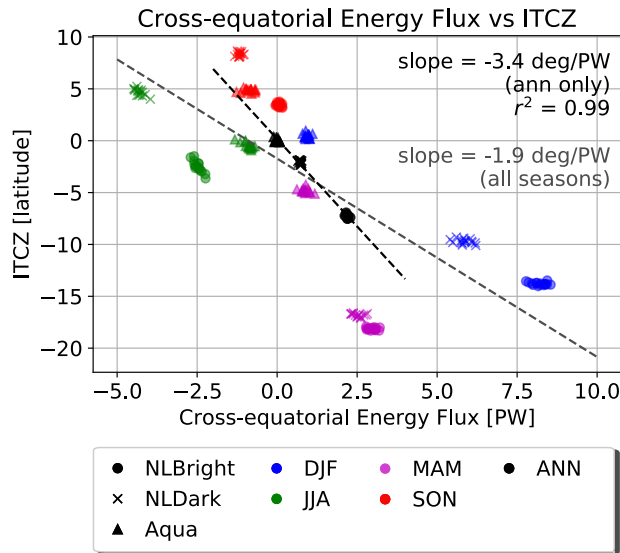
**Effect of Suppressing Terrestrial Evaporation on Surface Temperature and Specific Humidity in NorthlandDark vs. Aqua**



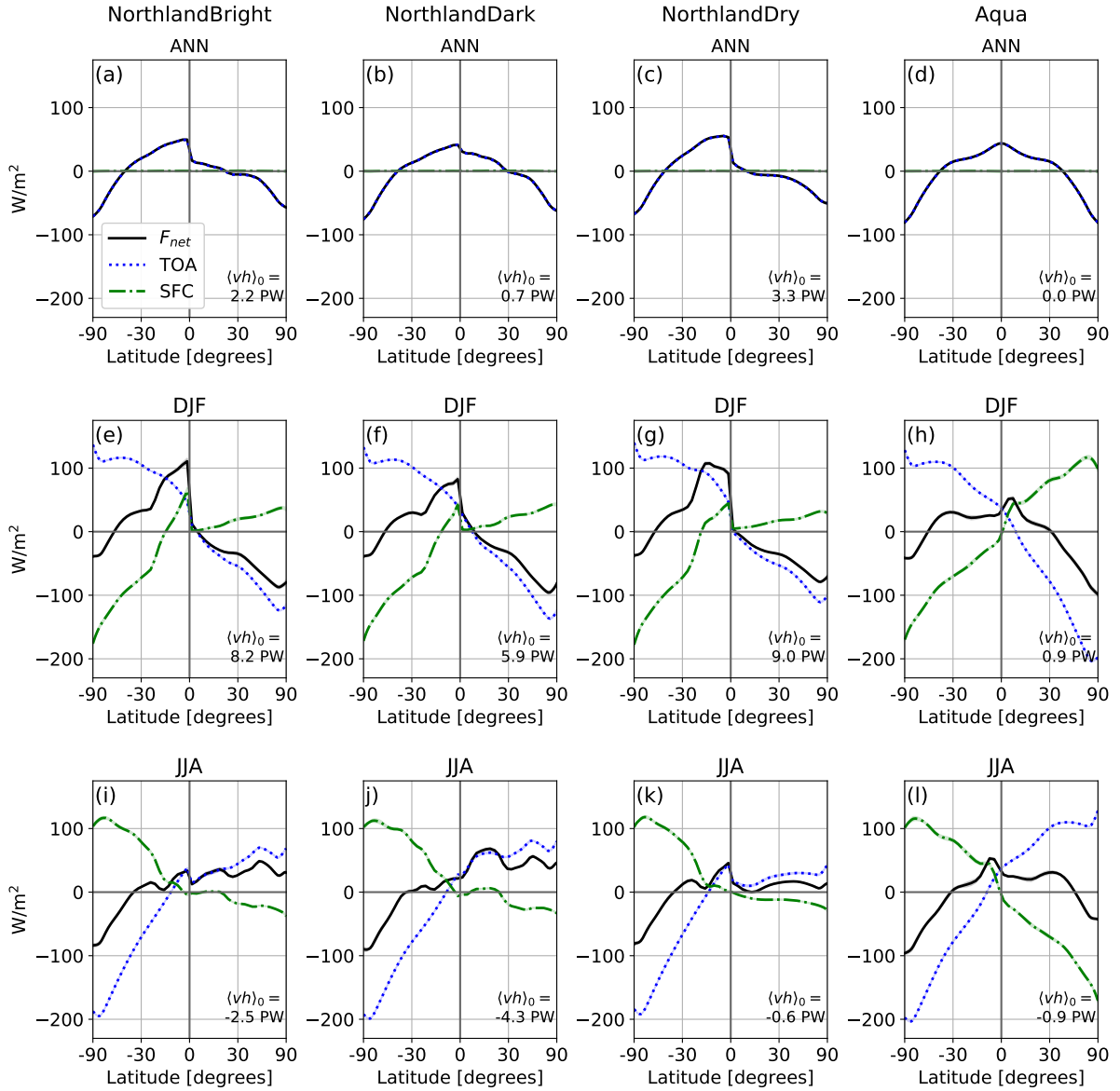
1179 FIG. 9. Change in surface temperature (left), change in latent heat flux (center), and percent change in zonal  
 1180 mean specific humidity (right) between NorthlandDark and Aqua. The annual mean change is shown in a-c,  
 1181 while the zonal-mean seasonal cycle is shown in d-e.



1182 FIG. 10. Top: zonal mean percent change in annual mean specific humidity for (a) NorthlandBright - Aqua  
 1183 and (b) NorthlandDark - Aqua. Middle: seasonal cycle of the zonal mean change in net SW absorbed at the  
 1184 surface for (c) NorthlandBright - Aqua and (d) NorthlandDark - Aqua. Bottom: ITCZ latitude calculated as the  
 1185 center of mass of zonal mean precipitation from 30°S to 30°N for NorthlandBright, NorthlandDark, and Aqua,  
 1186 where each dot represents a single month of the year.

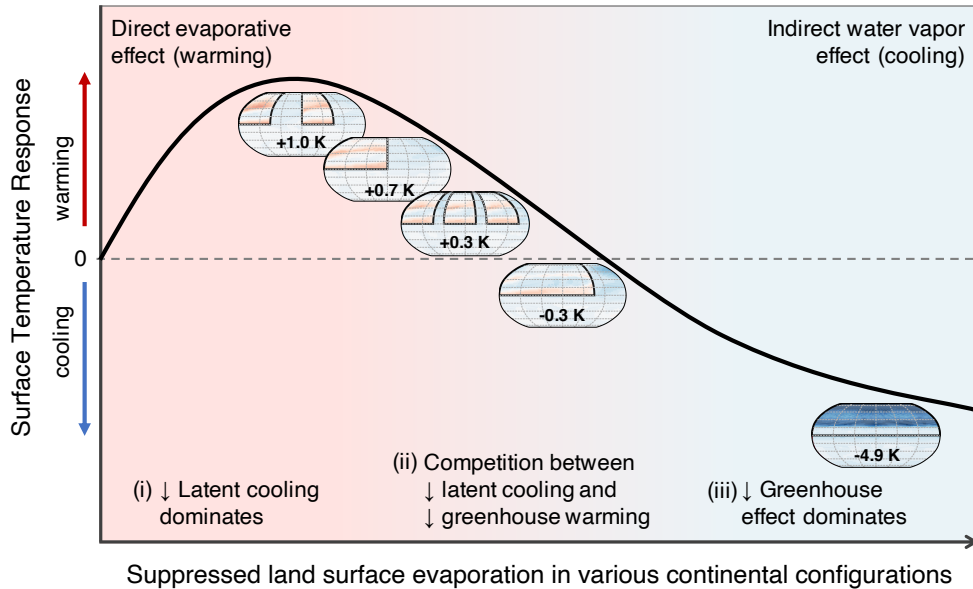


1187 FIG. 11. Relationship between the latitude of the ITCZ and the magnitude of cross-equatorial energy flux. The  
 1188 latitude of the ITCZ is calculated as the center of mass of precipitation between 30°S and 30°N; the magnitude  
 1189 of cross-equatorial energy flux is calculated as the magnitude of meridional atmospheric energy transport at the  
 1190 equator. Black markers indicate annual mean values, while blue, purple, green, and red markers indicate DJF,  
 1191 MAM, JJA, and SON averages, respectively. Circles show values for NorthlandBright, x for NorthlandDark,  
 1192 and triangles for Aqua. Each individual marker shows the seasonally averaged value for a single year of the time  
 1193 series. NorthlandDry is not included in the regression calculations here as the ITCZ effectively collapses over  
 1194 the continent.



1195 FIG. 12. Zonally averaged net TOA energy flux ( $TOA$ , blue dotted line), net surface energy flux ( $SFC$ ,  
1196 green dash-dot line), and the atmospheric column energy source ( $F_{net} = TOA - SFC$ ; black solid line) for the  
1197 annual mean (top row), DJF (middle row) and JJA (bottom row). NorthlandBright is shown in the first column,  
1198 NorthlandDark in the second, NorthlandDry in the third, and Aqua in the fourth. The total column integrated  
1199 cross-equatorial atmospheric energy transport (positive northwards) for each season is noted in the lower right  
1200 of each panel.





1201 FIG. 13. Schematic showing the surface temperature response to suppressed terrestrial evaporation for a vari-  
 1202 ety of NH continental configurations. Land area generally increases from left to right, though for a given total  
 1203 land area, larger continents sit farther to the right on the curve than smaller, more numerous continents. Qualita-  
 1204 tive locations of suppressing terrestrial evaporation on TwoPatchLand, NorthWestLand, ThreePatchLand, Three-  
 1205 QuarterLand, and Northland are shown by the maps of temperature change for each continental configuration,  
 1206 with the annual mean change in land surface temperature noted on each map.